Dynamics of streamwise rolls and streaks in turbulent wall-bounded shear flow

Brian F. Farrell[1] **and Petros J. Ioannou**[2]†

[1] Department of Earth and Planetary Sciences, Harvard University, Cambridge, MA 02138, USA

[2] Department of Physics, National and Kapodistrian University of Athens, Panepistimiopolis, Zografos, 15784, Greece

Streamwise rolls and accompanying streamwise streaks are ubiquitous in wall-bounded shear flows, both in natural settings, such as the atmospheric boundary layer, as well as in controlled settings, such as laboratory experiments and numerical simulations. The streamwise roll and streak structure has been associated with both transition from the laminar to the turbulent state and with maintenance of the turbulent state. This close association of the streamwise roll and streak structure with the transition to and maintenance of turbulence in wall-bounded shear flow has engendered intense theoretical interest in the dynamics of this structure. In this work, stochastic structural stability theory (SSST) is applied to the problem of understanding the dynamics of the streamwise roll and streak structure. The method of analysis used in SSST comprises a stochastic turbulence model (STM) for the dynamics of perturbations from the streamwise-averaged flow coupled to the associated streamwise-averaged flow dynamics. The result is an autonomous, deterministic, nonlinear dynamical system for evolving a second-order statistical mean approximation of the turbulent state. SSST analysis reveals a robust interaction between streamwise roll and streak structures and turbulent perturbations in which the perturbations are systematically organized through their interaction with the streak to produce Reynolds stresses that coherently force the associated streamwise roll structure. If a critical value of perturbation turbulence intensity is exceeded, this feedback results in modal instability of the combined streamwise roll/streak and associated turbulence complex in the SSST system. In this instability, the perturbations producing the destabilizing Reynolds stresses are predicted by the STM to take the form of oblique structures, which is consistent with observations. In the SSST system this instability exists together with the transient growth process. These processes cooperate in determining the structure of growing streamwise roll and streak. For this reason, comparison of SSST predictions with experiments requires accounting for both the amplitude and structure of initial perturbations as well as the influence of the SSST instability. Over a range of supercritical turbulence intensities in Couette flow, this instability equilibrates to form finite amplitude time-independent streamwise roll and streak structures. At sufficiently high levels of forcing of the perturbation field, equilibration of the streamwise roll and streak structure does not occur and the flow transitions to a time-dependent state. This time-dependent state is self-sustaining in the sense that it persists when the forcing is removed. Moreover, this self-sustaining state rapidly evolves toward a minimal representation of wall-bounded shear flow turbulence in which the dynamics is limited to interaction of the streamwise-averaged flow with a perturbation structure at one

† Email address for correspondence: pjioannou@phys.uoa.gr

streamwise wavenumber. In this minimal realization of the self-sustaining process, the time-dependent streamwise roll and streak structure is maintained by perturbation Reynolds stresses, just as is the case of the time-independent streamwise roll and streak equilibria. However, the perturbation field is maintained not by exogenously forced turbulence, but rather by an endogenous and essentially non-modal parametric growth process that is inherent to time-dependent dynamical systems.

Key words: parametric instability, transition to turbulence, turbulent transition

---

1. Introduction

In their experiments on transition to turbulence in boundary layers, Klebanoff and collaborators identified a prominent structure consisting of streamwise roll vortices and associated streamwise streaks (Klebanoff, Tidstrom & Sargent 1962). This streamwise roll and streak structure is commonly observed both in natural settings, such as the atmospheric boundary layer, as well as in controlled laboratory settings and numerical simulations. While the boundary in a simulation can be assumed analytically smooth and the flow in a laboratory experiment can be carefully prepared so that the level of background turbulence is kept small, most naturally occurring systems are substantially perturbed by upstream conditions and imperfections in the boundaries. This naturally occurring background turbulence is commonly simulated in laboratory experiments by using an upstream grid (Matsubara & Alfredsson 2001; Kurian & Fransson 2009). Interaction between streamwise roll and streak structures and this forced field of turbulence can strongly influence the dynamics of the streamwise roll and streak (Westin *et al.* 1994). One goal of this work is to improve understanding of the dynamics of the interaction between the streamwise roll and streak structure and background turbulence in transitional flows.

The Klebanoff modes are recognized to be precursor structures for the process of bypass transition in which these structures, despite being hydrodynamically stable in the sense of modal stability, instigate transition to a fully turbulent state. After transition, the streamwise roll and streak structure persists but becomes rapidly varying in space and time. This time-dependent streamwise roll and streak structure is believed to be involved in the process maintaining turbulence in shear flow (Kim, Kline & Reynolds 1971; Jiménez & Moin 1991; Hamilton, Kim & Waleffe 1995; Jiménez & Pinelli 1999; Schoppa & Hussain 2002). Further evidence for the involvement of this structure in maintaining the turbulent state is provided by minimal channel simulations in which the streamwise roll and streak structure is observed to be in a self-sustaining time-dependent state (Hamilton *et al.* 1995; Waleffe 1995, 1997; Jiménez & Pinelli 1999). A second goal of this work is to improve understanding of the dynamics of the streamwise roll and streak structure in the self-sustaining process (SSP).

We turn first to the robust observation of the streamwise roll and streak structure in boundary layers prior to transition to turbulence, which presented a problem historically because this structure is not unstable in planar shear flow. The robust appearance of this structure was first explained by appeal to the lift-up mechanism (Ellingsen & Palm 1975; Landahl 1980). This insight was later advanced by recognition of the connection between the lift-up mechanism and the non-normality of the associated dynamical operator. Non-normal operator analysis confirmed that the optimally growing perturbations, over sufficiently long time intervals, are

streamwise rolls and streaks (Butler & Farrell 1992; Reddy & Henningson 1993; Trefethen *et al.* 1993; Schmid & Henningson 2001). However, for short optimizing times the linear optimal perturbations are oblique structures (Farrell & Ioannou 1993*a*,*b*; Jovanovic & Bamieh 2005) and, interestingly, oblique perturbations have also been identified as nonlinear optimal structures for transition in Couette flow (Monokrousos *et al.* 2011). Consistent with the optimality of these structures, both the long time optimal streamwise roll and streak and the short time optimal oblique perturbations have been convincingly seen in observations and simulations (Sirovich, Ball & Keefe 1990; Adrian 2007; Hutchins & Marusic 2007; Wu & Moin 2009) and also shown to be essentially related to the non-normality of shear flow dynamics (Kim & Lim 2000; Schoppa & Hussain 2002).

The mechanism of non-normal growth has been clarified and its importance in bypass transition and maintenance of turbulence is now widely accepted. However, the route by which non-normality leads to the formation of streamwise rolls and streaks in turbulent wall-bounded shear flows, and the part played by this coherent structure in both the transition to turbulence and maintenance of the turbulent state remains to be determined comprehensively.

Appearance of the streamwise roll and streak in shear flow could result from its being the most amplified outcome of a linear initial value problem or from a nonlinear mechanism in which turbulent Reynolds stresses generate and amplify this structure. These are fundamentally related explanations because both the linear non-normal growth and the nonlinear Reynolds stress interaction mechanisms exploit the same non-normal lift-up mechanism.

The linear non-normal lift-up mechanism can be induced by introducing a streamwise roll perturbation directly into the flow, perhaps by using a trip or other device. Using non-normal operator analysis, Andersson, Berggren & Henningson (1999) and Luchini (2000) identified the streamwise roll and streak in developing boundary layers as an optimally spatially amplifying structure forced at the leading edge. A related approach is to force the flow stochastically, with the stochastic forcing regarded as modelling external disturbances (Farrell & Ioannou 1993*d*,*e*, 1994; Bamieh & Dahleh 2001; Jovanovic & Bamieh 2005; Hoepffner & Brandt 2008; Gayme *et al.* 2010; Hwang & Cossu 2010*b*). In these stochastically forced models, the streamwise roll and streak structure is envisioned to arise from excitation of optimal or near-optimal perturbations by the forcing.

The nonlinear non-normal mechanism can result from streamwise roll forcing by interacting discrete oblique waves and/or Tollmien–Schlichting waves (Benney 1960, 1984; Jang, Benney & Gran 1986; Schmid & Henningson 1992; Reddy *et al.* 1998; Brandt, Henningson & Ponziani 2002) and from Reynolds stresses associated with marginally stable critical layers (Hall & Sherwin 2010).

It may be thought that the linear mechanism, which is first order in the perturbation amplitude, should dominate over the second-order nonlinear mechanism because perturbation amplitudes in boundary layers are typically small. However, Berlin & Henningson (1999), in simulations of transition in a parallel flow approximation to the Blasius boundary layer, found that streaks of the same order of magnitude are generated by linear and nonlinear mechanisms for an initial random perturbation field with 1 % velocity fluctuations. Dominance of the nonlinear mechanism in a boundary layer subjected to free stream turbulence (FST) was also found by Jacobs & Durbin (2001). Perhaps the most compelling evidence for the importance of the nonlinear growth mechanism is the observation that streamwise roll initial conditions decay in amplitude if FST levels are not sufficiently high (Alfredsson & Matsubara 1996;

Bakchinov, Katasonov & Kozlov 1997; Westin *et al.* 1998), while these structures grow downstream in the presence of moderate levels of FST (Westin *et al.* 1994). Moreover, both the linear and nonlinear mechanisms can participate in streamwise roll and streak growth with the linear providing the initial growth and the nonlinear becoming important near the time of transition (Brandt, Schlatter & Henningson 2004). In this work we show how the linear and the nonlinear mechanisms cooperate to form an unstable structure exploiting both mechanisms. Indeed, the experiments discussed above suggest that such a cooperative instability may often be involved in formation of the streamwise roll and streak.

However, such an instability must differ qualitatively from the familiar hydrodynamic modal instability because the streamwise roll and streak is exponentially stable in that sense. The streamwise roll provides a powerful mechanism for forming and amplifying streamwise streaks in shear flow through the lift-up mechanism. However, in the absence of feedback between the amplifying streak and streamwise roll this powerful growth mechanism does not result in instability. Owing to the large streak growth produced by a streamwise roll perturbation, placing even a weak coupling of the streak back to the roll, such as is provided by a small spanwise frame rotation, produces destabilization (Komminaho, Lundbladh & Johansson 1996; Farrell & Ioannou 2008*a*). The close association between the growing streak and oblique waves suggests that these waves are involved in providing the feedback destabilizing the streamwise roll and streak in the presence of turbulent perturbations (Schoppa & Hussain 2002). If we observe a turbulent shear flow in the cross-stream/spanwise plane at a fixed streamwise location, we see that, at any instance of time, there is a substantial Reynolds stress forcing tending to form streamwise rolls. The problem is that this streamwise roll forcing is not systematic and so it vanishes in temporal or streamwise average and therefore does not produce a coherent forcing of the streamwise roll circulation. However, streamwise roll forcing by the Reynolds stresses could, at least in principle, be organized by the presence of a streak to produce the coherent positive feedback between the streak and roll required for instability. We demonstrate that this mechanism does result in instability by deriving a dynamical system for the statistical mean turbulent state at second order from which we obtain the unstable streamwise roll/streak/turbulence mode. The mechanism of this instability is illustrated in figure 1.

This instability of interaction between the turbulence and the streamwise roll and streak differs from the mechanism of transient growth of an initial streamwise roll in that the streamwise roll is being continually forced by the perturbations. However, a streamwise roll resulting from an optimal perturbation would generally excite an eigenmode of this interaction dynamics thereby transforming the transiently growing streak, and its decaying streamwise roll, into a continuously growing mode. When so initiated by a finite optimal streamwise roll initial condition, the streamwise roll and streak instability would, at least initially, inherit the spatial scale of the optimal rather than manifest the scale of the maximal instability.

In order to construct a theory for this instability we require a method of analysis applicable to turbulence/mean flow interaction. The analysis method we use is based on a dynamical system for evolving a second-order approximation of the turbulent state. We refer to this dynamical system as the stochastic structural stability theory (SSST) system. This method for analysing the dynamics of turbulence was developed to study the phenomenon of spontaneous jet formation in planetary atmospheres (Farrell & Ioannou 2003, 2007, 2008*a*; Bakas & Ioannou 2011) and has also been applied to the problem of spontaneous jet formation from drift wave
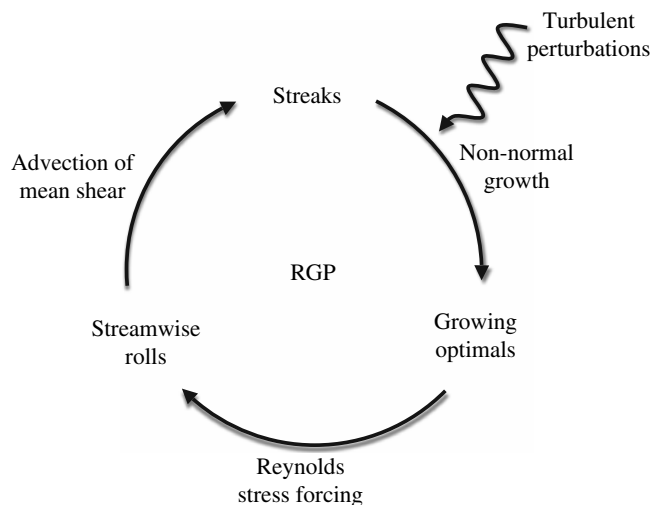
FIGURE 1. The roll/streak growth process (RGP) in which turbulent perturbations are organized by the streak to produce Reynolds stresses collocated to force the associated streamwise roll, which in turn amplifies the streak via the lift-up mechanism.

turbulence in magnetic fusion devices (Farrell & Ioannou 2009). In SSST, the turbulence is simulated using a stochastic turbulence model (STM) (Farrell & Ioannou 1993c, 1996a; DelSole & Farrell 1996; Bamieh & Dahleh 2001; DelSole 2004; Gayme et al. 2010). The STM provides an evolution equation for the streamwise-averaged perturbation covariance from which the Reynolds stresses can be obtained. Coupling this equation to an evolution equation for the streamwise-averaged flow produces a nonlinear dynamical system for the co-evolution of the streamwise-averaged flow and its associated perturbation covariance: this is the SSST system. Related second-order closures have recently been proposed by Marston, Conover & Schneider (2008), Marston (2010), Tobias, Dagon & Marston (2011) and Srinivasan & Young (2012).

The SSST equations constitute an autonomous and deterministic system in the variables of the three components of the streamwise-averaged flow and the streamwise-averaged perturbation covariance. While hydrodynamic instability is supported by the SSST dynamical system, the primary instability in SSST dynamics has no counterpart in the stability theory of laminar flow; it is rather the new form of cooperative streamwise roll and streak plus turbulence instability described above. We refer to this cooperative instability as structural instability to distinguish it from hydrodynamic instability. This new instability is referred to as structural because when the equilibrium state is unstable the system bifurcates to a new state on a distinct attractor. The SSST equations incorporate the nonlinear feedback between the evolving streamwise roll and streak and its consistent field of turbulence which may produce equilibration to stable states. These equilibrium states differ from exact coherent structures, as in Nagata (1990), in being both stable and maintained by interaction with an incoherent perturbation field. However, as the perturbation forcing increases, the SSST equilibrium states ultimately lose stability. The resulting instability leads to transition to a time-dependent state, which we show self-sustains on removal of the exogenous forcing.

Self-sustaining states have been the subject of numerous studies and the primary mechanism advanced to explain how these states are maintained is a cycle in which the streamwise roll is forced by Reynolds stresses associated with modal instability of
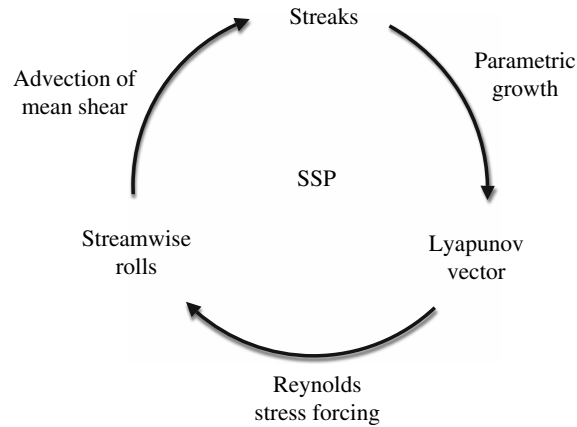
FIGURE 2. The SSP in which a time-dependent streak induces parametric growth of perturbations which produce Reynolds stresses that amplify the associated streamwise roll and maintain the streak via the lift-up mechanism.

the streak (Hamilton *et al.* 1995; Waleffe 1997). The mechanism maintaining the self-sustaining state in SSST is similar in that perturbation Reynolds stress forcing of the highly non-normal streamwise roll and streak structure is central. However, it differs in that an essentially time-dependent, non-normal, parametric growth mechanism, rather than modal instability, is responsible for maintaining the perturbation field (Farrell & Ioannou 1996*b*, 1999; Pedlosky & Thomson 2003; Poulin, Flierl & Pedlosky 2003; Farrell & Ioannou 2008*b*; Poulin, Flierl & Pedlosky 2010). This self-sustaining cycle is illustrated in figure 2.

We begin in §2 by formulating the dynamics of the interaction between perturbations and streamwise-averaged flows using a stochastic parameterization for the perturbation–perturbation nonlinearity and the external forcing. In §3 we present the SSST system, which is a second-order closure of this dynamics. In §4 we introduce the turbulence/mean flow interaction instability and study the bifurcation properties of the SSST system. In §5 we study the dynamics underlying the growth and nonlinear equilibration of the streamwise roll and streak instability. In §6 we study the growth of optimal perturbations in the SSST system and extend our results to a parallel flow approximation of the Blasius boundary layer. In §7 we study transition to the self-sustaining state of the SSST system. In §8 we show that this self-sustaining state leads to a minimal representation of turbulence. In §9 we examine the dynamics underlying this self-sustaining state.

2. Formulation of the dynamics of the interaction between perturbations and streamwise-averaged flows

Averaging in the streamwise, x, direction is denoted with a bar, and streamwise-averaged quantities are indicated by uppercase characters; spanwise, z, averages are denoted with square brackets, $[\cdot]$, and ensemble averages with angle brackets, $\langle\cdot\rangle$. Velocity fields are decomposed into streamwise-averaged components and perturbations (indicated lowercase) so that the total streamwise velocity in the x direction is $U(y, z, t) + u(x, y, z, t)$, the cross-stream velocity in the y direction is $V(y, z, t) + v(x, y, z, t)$, the spanwise velocity in the z direction is $W(y, z, t) + w(x, y, z, t)$ and the pressure is $P(y, z, t) + p(x, y, z, t)$. In vector form $\boldsymbol{U} = (U, V, W)$ and $\boldsymbol{u} = (u, v, w)$. Consider, as in a Couette flow, a channel in which the walls at $y = \pm L_y$

move with velocity in the streamwise direction $\pm U_0$, respectively. Impose periodic boundary conditions in x and z, with periodicity L_x and L_z, respectively. Non-dimensionalize distance with the cross-stream channel half-width, L_y, and time with L_y/U_0, and define the Reynolds number as $R = U_0 L_y/\nu$, with ν the kinematic viscosity.

Consider the flow of a unit density fluid obeying the non-divergent Navier–Stokes equations:

$$\boldsymbol{u}_t + \boldsymbol{U} \cdot \nabla \boldsymbol{u} + \boldsymbol{u} \cdot \nabla \boldsymbol{U} + \nabla p - \Delta \boldsymbol{u}/R = -(\boldsymbol{u} \cdot \nabla \boldsymbol{u} - \overline{\boldsymbol{u} \cdot \nabla \boldsymbol{u}}) + \boldsymbol{e}, \qquad (2.1a)$$

$$\boldsymbol{U}_t + \boldsymbol{U} \cdot \nabla \boldsymbol{U} + \nabla P - \Delta \boldsymbol{U}/R = -\overline{\boldsymbol{u} \cdot \nabla \boldsymbol{u}}, \qquad (2.1b)$$

$$\nabla \cdot \boldsymbol{U} = 0, \quad \nabla \cdot \boldsymbol{u} = 0. \qquad (2.1c)$$

In the perturbation equation $(2.1a)$ the nonlinear terms have been augmented by an explicit external perturbation forcing, $\boldsymbol{e}$. A stochastic parameterization is introduced to account for both the perturbation external forcing and the perturbation–perturbation interactions, $\boldsymbol{u} \cdot \nabla \boldsymbol{u} - \overline{\boldsymbol{u} \cdot \nabla \boldsymbol{u}}$. With this parameterization, the perturbation equation $(2.1a)$ becomes

$$\boldsymbol{u}_t + \boldsymbol{U} \cdot \nabla \boldsymbol{u} + \boldsymbol{u} \cdot \nabla \boldsymbol{U} + \nabla p - \Delta \boldsymbol{u}/R = \boldsymbol{E}. \qquad (2.2)$$

Perturbation equation (2.2), coupled with the mean flow equation, $(2.1b)$, form a nonlinear system which we will show captures the fundamental behaviour of wall-bounded shear flow turbulence.

It is convenient to express (2.2) in terms of cross-stream velocity v and cross-stream vorticity, $\eta = \partial_z u - \partial_x w$. The equation then takes the form (cf. Schmid & Henningson 2001):

$$\Delta v_t + U\Delta v_x + U_{zz}v_x + 2U_z v_{xz} - U_{yy}v_x - 2U_z w_{xy} - 2U_{yz}w_x - \Delta\Delta v/R = \Delta E_v, \quad (2.3a)$$

$$\eta_t + U\eta_x - U_z v_y + U_{yz}v + U_y v_z + U_{zz}w - \Delta\eta/R = E_\eta \qquad (2.3b)$$

where E_v and E_η are the stochastic excitation in these variables. In (2.3), interaction of the perturbation velocities with W and V has been neglected because these velocities are much smaller than U. The spanwise and streamwise perturbation velocities are obtained from the cross-stream velocity and vorticity as follows:

$$\Delta_2 w = -v_{yz} - \eta_x, \quad \Delta_2 u = -v_{yx} + \eta_z, \qquad (2.4)$$

with $\Delta_2 \equiv \partial_{xx}^2 + \partial_{zz}^2$.

The mean flow equation $(2.1b)$ can be written as

$$U_t = U_y \Psi_z - U_z \Psi_y - \partial_y \overline{uv} - \partial_z \overline{uw} + \Delta_1 U/R, \qquad (2.5a)$$

$$\Delta_1 \Psi_t = (\partial_{yy} - \partial_{zz})(\Psi_y \Psi_z - \overline{vw}) - \partial_{yz}(\Psi_y^2 - \Psi_z^2 + \overline{w^2} - \overline{v^2}) + \Delta_1 \Delta_1 \Psi/R. \quad (2.5b)$$

In $(2.5b)$, $\Delta_1 \equiv \partial_{yy}^2 + \partial_{zz}^2$; V and W are expressed in terms of the streamfunction, Ψ, as $V = -\Psi_z$ and $W = \Psi_y$.

In $(2.5a)$, the streamwise mean velocity, U, is forced by the term, $-\partial_y \overline{uv} - \partial_z \overline{uw}$, which is the streamwise component of the perturbation Reynolds stress divergence, and by the term, $U_y \Psi_z - U_z \Psi_y$, the first part of which is the familiar lift-up mechanism. In $(2.5b)$, the Reynolds stress term, $-(\partial_{yy} - \partial_{zz})\overline{vw} - \partial_{yz}(\overline{w^2} - \overline{v^2})$, provides the streamwise roll forcing generating streamwise vorticity, $\Omega_x = \Delta_1 \Psi$, while the mean flow advection term, $(\partial_{yy} - \partial_{zz})\Psi_y \Psi_z - \partial_{yz}(\Psi_y^2 - \Psi_z^2)$, redistributes Ω_x.

3. Formulation of the SSST dynamics

In the previous section we have simplified the perturbation dynamics by using a stochastic parameterization for the quadratic perturbation nonlinearity and the background turbulence forcing. For each realization of the stochastic excitation the perturbation equations (2.3) provide a single realization of the perturbation field, which interacts with the streamwise-averaged flow governed by (2.5). However, the streamwise-averaged flow interacts with streamwise localized structures, separated on average by the decorrelation scale of the perturbation field in the streamwise direction. The net effect of these localized structures on the streamwise-averaged flow can be obtained from an ensemble of realizations of the perturbation field. The dynamics of the interaction of an infinite ensemble with the mean flow is used in the SSST dynamics, which we now formulate.

Fourier expand the perturbation fields in x:

$$v = \sum_k \hat{v}_k(y, z, t)\mathrm{e}^{\mathrm{i}kx}, \quad \eta = \sum_k \hat{\eta}_k(y, z, t)\mathrm{e}^{\mathrm{i}kx}, \tag{3.1}$$

with a finite number of $k > 0$ and the $k = 0$ streamwise wavenumber excluded. In matrix form, the perturbation evolution equations for each streamwise Fourier component, discretized in y and z on $N = N_y N_z$ points, are

$$\frac{\mathrm{d}\hat{\boldsymbol{\phi}}_k}{\mathrm{d}t} = \boldsymbol{A}_k(\boldsymbol{U})\hat{\boldsymbol{\phi}}_k + \boldsymbol{\epsilon}_k, \tag{3.2}$$

where

$$\hat{\boldsymbol{\phi}}_k = \begin{pmatrix} \hat{\boldsymbol{v}}_k \\ \hat{\boldsymbol{\eta}}_k \end{pmatrix} \tag{3.3}$$

is the perturbation state in which each variable is considered as a column vector, and $\boldsymbol{U}$ is a matrix with diagonal elements the streamwise-averaged streamwise velocity. The stochastic term, $\boldsymbol{\epsilon}_k$, on the right-hand side of (3.2), which parameterizes the neglected nonlinear terms and the external excitation at wavenumber k, will be specified below. The matrix $\boldsymbol{A}_k$ is

$$\boldsymbol{A}_k(\boldsymbol{U}) = \begin{pmatrix} \boldsymbol{L}_{OS} & \boldsymbol{L}_{C_1} \\ \boldsymbol{L}_{C_2} & \boldsymbol{L}_{SQ} \end{pmatrix}, \tag{3.4}$$

with

$$\boldsymbol{L}_{OS} = \boldsymbol{\Delta}^{-1}(-\mathrm{i}k\boldsymbol{U}\boldsymbol{\Delta} + \mathrm{i}k(\boldsymbol{U}_{yy} - \boldsymbol{U}_{zz}) - 2\mathrm{i}k\boldsymbol{U}_z\partial_z$$
$$- 2\mathrm{i}k(\boldsymbol{U}_z\partial^3_{yyz} + \boldsymbol{U}_{yz}\partial^2_{yz})\boldsymbol{\Delta}_2^{-1} + \boldsymbol{\Delta}\boldsymbol{\Delta}/R), \tag{3.5a}$$

$$\boldsymbol{L}_{C_1} = 2k^2\boldsymbol{\Delta}^{-1}\left(\boldsymbol{U}_z\partial_y + \boldsymbol{U}_{yz}\right)\boldsymbol{\Delta}_2^{-1}, \tag{3.5b}$$

$$\boldsymbol{L}_{C_2} = \boldsymbol{U}_z\partial_y - \boldsymbol{U}_y\partial_z - \boldsymbol{U}_{yz} + \boldsymbol{U}_{zz}\partial^2_{yz}\boldsymbol{\Delta}_2^{-1}, \tag{3.5c}$$

$$\boldsymbol{L}_{SQ} = -\mathrm{i}k\boldsymbol{U}\boldsymbol{\Delta} + \mathrm{i}k\boldsymbol{U}_{zz}\boldsymbol{\Delta}_2^{-1} + \boldsymbol{\Delta}/R. \tag{3.5d}$$

In (3.5) we denote the matrix approximations of the operators by bold symbols. $\boldsymbol{\Delta}^{-1}$ and $\boldsymbol{\Delta}_2^{-1}$ are the inverses of the matrix Laplacians, $\boldsymbol{\Delta}$ and $\boldsymbol{\Delta}_2$, which are rendered invertible by enforcing the boundary conditions. The boundary conditions satisfied

by the Fourier amplitudes of the perturbation fields are periodicity in x and z and $\hat{v}_k = \partial_y \hat{v}_k = \hat{\eta}_k = 0$ at $y = \pm 1$.

In terms of the perturbation state, $\hat{\boldsymbol{\phi}}_k$, the perturbation velocities are

$$\hat{\boldsymbol{u}}_k = \boldsymbol{L}_u^k \hat{\boldsymbol{\phi}}_k, \quad \hat{\boldsymbol{v}}_k = \boldsymbol{L}_v^k \hat{\boldsymbol{\phi}}_k, \quad \hat{\boldsymbol{w}}_k = \boldsymbol{L}_w^k \hat{\boldsymbol{\phi}}_k, \tag{3.6}$$

with the matrices given by

$$\boldsymbol{L}_u^k = [-ik\boldsymbol{\Delta}_2^{-1}\partial_y \quad -\boldsymbol{\Delta}_2^{-1}\partial_z], \tag{3.7a}$$

$$\boldsymbol{L}_v^k = [\boldsymbol{I} \ \boldsymbol{0}], \tag{3.7b}$$

$$\boldsymbol{L}_w^k = [-\boldsymbol{\Delta}_2^{-1}\partial_{yz}^2 \quad -ik\boldsymbol{\Delta}_2^{-1}]. \tag{3.7c}$$

The stochastic term, $\boldsymbol{\epsilon}_k$, on the right-hand side in (3.2) is expressed as $f_k \boldsymbol{F}_k \boldsymbol{\xi}(t)$ where $\boldsymbol{\xi}(t)$ is a $2N$ column vector of random variables, $\boldsymbol{F}_k$ is a matrix that determines the spatial correlation of the forcing, and f_k is a scalar used to control the amplitude of the forcing. The stochastic vector, $\boldsymbol{\xi}(t)$, is a Gaussian random process which has zero mean and is delta correlated in time:

$$\langle \boldsymbol{\xi}(t)\boldsymbol{\xi}^\dagger(s) \rangle = \boldsymbol{I}\delta(t-s). \tag{3.8}$$

In the above, † denotes Hermitian transpose and $\boldsymbol{I}$ is the identity matrix.

Consider an ensemble of perturbation fields obeying (3.2). The ensemble average perturbation covariance, $\boldsymbol{C}_k = \langle \hat{\boldsymbol{\phi}}_k \hat{\boldsymbol{\phi}}_k^\dagger \rangle$, can be shown (cf. Farrell & Ioannou 1993e) to evolve according to the time-dependent Lyapunov equation:

$$\frac{\mathrm{d}\boldsymbol{C}_k}{\mathrm{d}t} = \boldsymbol{A}_k(\boldsymbol{U})\boldsymbol{C}_k + \boldsymbol{C}_k\boldsymbol{A}_k^\dagger(\boldsymbol{U}) + f_k^2\boldsymbol{Q}_k, \tag{3.9}$$

in which

$$\boldsymbol{Q}_k = \boldsymbol{F}_k\boldsymbol{F}_k^\dagger. \tag{3.10}$$

Equation (3.9) is the autonomous and deterministic STM that provides an evolution equation for the perturbation covariance from which all second-order turbulence statistics can be determined. For a given streamwise-averaged velocity, $\boldsymbol{U}$, the STM provides accurate second-order perturbation statistics (Farrell & Ioannou 1998b; Laval, Dubrulle & McWilliams 2003) and it has been widely used to model the dynamics of turbulence in channel flows (Farrell & Ioannou 1993e, 1998a; Jovanovic & Bamieh 2005; Hoepffner & Brandt 2008; Hwang & Cossu 2010a; Gayme *et al.* 2010). The STM has also been instrumental in advancing robust control of channel flow turbulence (Bewley & Liu 1998; Farrell & Ioannou 1998b; Hogberg, Bewley & Henningson 2003; Kim & Bewley 2007). In addition, the STM has been used to obtain the midlatitude atmospheric jet perturbation structure (Farrell & Ioannou 1995; Zhang & Held 1999; DelSole 2004; Marston *et al.* 2008).

The stochastic forcing used in the STM is generally taken to be approximately spatially white in order to maintain a broad spectrum of perturbations typical of turbulence (Farrell & Ioannou 1993e; Bamieh & Dahleh 2001). Similar to its role in the above works, the role of the stochastic forcing in this work is to produce a broadband field of perturbations rather than to duplicate a particular physical source of turbulence such as wall roughness or FST that results from an upstream grid and our predictions may suffer from this simplification. However, we believe that the essential dynamics are captured with a uniformly distributed broadband stochastic forcing, although this remains to be verified in future work.

When turbulence was forced using an upstream grid by Westin *et al.* (1994), the FST resulting filled the test section of their boundary layer with a broad spectrum of perturbations at a nearly constant turbulence intensity of around $Tu = 1.5\%$. In their simulations, Wu & Moin (2009) used an upstream isotropic forcing to produce patches of turbulence that propagate downstream, reaching values of $Tu = 1$–3% in the region of streak growth. These levels of FST exceed the FST levels that can be achieved in the test sections of low-turbulence wind tunnels by as much as two orders of magnitude. In this study we use stochastic forcing producing perturbation velocities corresponding to turbulent intensities in the range 1–3%, which are typical of experiments in transitional boundary layer flows.

In this work, the stochastic forcing maintaining the turbulence is chosen so that each degree of freedom is excited equally in energy. As will be explained below, this is accomplished by choosing:

$$\boldsymbol{Q}_k = \boldsymbol{M}_k^{-1}, \tag{3.11}$$

where, using the definitions of the velocity operators (3.6),

$$\boldsymbol{M}_k = \frac{1}{4N_y N_z} \left(\boldsymbol{L}_u^{k\dagger} \boldsymbol{L}_u^k + \boldsymbol{L}_v^{k\dagger} \boldsymbol{L}_v^k + \boldsymbol{L}_w^{k\dagger} \boldsymbol{L}_w^k \right). \tag{3.12}$$

It follows that the volume-averaged perturbation energy density, at streamwise wavenumber k is

$$E_k = \hat{\boldsymbol{\phi}}_k^{\dagger} \boldsymbol{M}_k \hat{\boldsymbol{\phi}}_k. \tag{3.13}$$

Owing to the equalities:

$$\langle E_k \rangle = \langle \hat{\boldsymbol{\phi}}_k^{\dagger} \boldsymbol{M}_k \hat{\boldsymbol{\phi}}_k \rangle = \text{trace}(\boldsymbol{M}_k \langle \hat{\boldsymbol{\phi}}_k \hat{\boldsymbol{\phi}}_k^{\dagger} \rangle) = \text{trace}(\boldsymbol{M}_k \boldsymbol{C}_k), \tag{3.14}$$

the ensemble average energy density of the perturbation field is obtained by multiplying the covariance, $\boldsymbol{C}_k$, by $\boldsymbol{M}_k$.

The choice of forcing covariance given in (3.11) can be motivated by noticing that if the dynamics were only a scale-independent linear damping, so that $\boldsymbol{A} = -r\boldsymbol{I}$, then multiplying (3.9) by $\boldsymbol{M}_k$, and choosing $\boldsymbol{Q}_k = \boldsymbol{M}_k^{-1}$, we obtain a steady state with covariance $\boldsymbol{C}_k = \boldsymbol{M}_k^{-1}/(2r)$ and as a result $\boldsymbol{M}_k \boldsymbol{C}_k = \boldsymbol{I}/(2r)$, which shows that choosing $\boldsymbol{Q}_k = \boldsymbol{M}_k^{-1}$ results in each degree of freedom being equally excited in energy.

This choice of perturbation forcing distributed uniformly in energy has the advantage both of approximating the broadband nature of turbulent fluctuations and of removing the stochastic forcing structure from consideration as a variable in the problem.

In this work, the stochastic forcing covariance, $\boldsymbol{Q}_k$, is scaled to maintain at equilibrium a volume-averaged root mean square (r.m.s.) perturbation velocity, 1% of the maximum velocity, when it is used to force the Couette flow profile with $f_k = 1$ in (3.9). Explicitly, $\boldsymbol{Q}_k$ is scaled so that $\sqrt{2\langle E_k \rangle} = 0.01$, where $\langle E_k \rangle$ is given by (3.13) and $\boldsymbol{C}_k$ solves (3.9) with $U = y$, $f_k = 1$ and the left-hand side set to zero. The explicit parameter, f_k, serves as the primary control parameter in this work. This parameter controls the percentage volume-averaged turbulence intensity, defined and denoted as $\{I_u\} = 100\sqrt{2\langle E_k \rangle/3}$. For the Couette flow profile and with the chosen normalization of the forcing, $\{I_u\} = f_k/\sqrt{3}$. The commonly available measure of turbulence in experiments is the FST intensity, Tu. While these measures are not the same, they correspond closely as measures of turbulence intensity.

The covariances, $\boldsymbol{C}_k$, which evolve according to STM dynamics (3.9), provide the Reynolds stresses for the mean flow equation (2.5) under the ergodic assumption of equating streamwise and ensemble averages. For example, it is assumed that the Reynolds stress component $\overline{uv} = \langle uv \rangle$. This implies that this Reynolds stress component, at streamwise wavenumber k, is equal to $\mathrm{Re}(\overline{\boldsymbol{uv}}|_k)$, where Re denotes the real part and the vector symbol $\overline{\boldsymbol{uv}}|_k$ is defined as

$$
\begin{aligned}
\overline{\boldsymbol{uv}}|_k &\equiv \tfrac{1}{2}\mathrm{diag}(\langle \hat{\boldsymbol{u}}_k \hat{\boldsymbol{v}}_k^{\dagger} \rangle) \\
&= \tfrac{1}{2}\mathrm{diag}(\langle \boldsymbol{L}_u^k \hat{\boldsymbol{\phi}}_k \,(\boldsymbol{L}_v^k \hat{\boldsymbol{\phi}}_k)^{\dagger} \rangle) \\
&= \tfrac{1}{2}\mathrm{diag}(\boldsymbol{L}_u^k \boldsymbol{C}_k \boldsymbol{L}_v^{k\dagger}).
\end{aligned}
\tag{3.15}
$$

In (3.15), $\mathrm{diag}(\boldsymbol{B})$ denotes the vector with elements the diagonal of the matrix $\boldsymbol{B}$. The total Reynolds stress is the sum over the contributions from the streamwise harmonics:

$$
\overline{uv} = \sum_k \mathrm{Re}(\overline{\boldsymbol{uv}}|_k).
\tag{3.16}
$$

The streamwise-averaged flow equation (2.5) can be expressed concisely in the form:

$$
\frac{\mathrm{d}\boldsymbol{\Gamma}}{\mathrm{d}t} = \boldsymbol{G}(\boldsymbol{\Gamma}) + \sum_k \mathrm{Re}(\boldsymbol{L}_{RS}\boldsymbol{C}_k),
\tag{3.17}
$$

where $\boldsymbol{\Gamma} \equiv [\boldsymbol{U},\ \boldsymbol{\Psi}]^{\mathrm{T}}$ and $\boldsymbol{C}_k$ is the covariance at wavenumber, k. In (3.17), G is

$$
\boldsymbol{G}(\boldsymbol{\Gamma}) = \begin{pmatrix} \partial_y \boldsymbol{U} \circ \partial_z \boldsymbol{\Psi} - \partial_z \boldsymbol{U} \circ \partial_y \boldsymbol{\Psi} + \Delta_1 \boldsymbol{U}/R \\ \Delta_1^{-1}[(\partial_{yy} - \partial_{zz})\partial_y \boldsymbol{\Psi} \circ \partial_z \boldsymbol{\Psi} - \partial_{yz}(\partial_y \boldsymbol{\Psi} \circ \partial_y \boldsymbol{\Psi} - \partial_z \boldsymbol{\Psi} \circ \partial_z \boldsymbol{\Psi}) + \Delta_1 \Delta_1 \boldsymbol{\Psi}/R] \end{pmatrix}.
\tag{3.18}
$$

In the above equation $\circ$ denotes the Hadamard product. The forcing of $\boldsymbol{\Gamma}$ by the Reynolds stresses at the wavenumber k is

$$
\boldsymbol{L}_{RS}\boldsymbol{C}_k = \begin{pmatrix} -\partial_y \overline{\boldsymbol{uv}}|_k - \partial_z \overline{\boldsymbol{uw}}|_k \\ \Delta_1^{-1}[-(\partial_{yy} - \partial_{zz})\overline{\boldsymbol{vw}}|_k - \partial_{yz}(\overline{\boldsymbol{w}^2}|_k - \overline{\boldsymbol{v}^2}|_k)] \end{pmatrix},
\tag{3.19}
$$

where $\overline{\boldsymbol{uv}}|_k$ is given in (3.15) and

$$
\overline{\boldsymbol{uw}}|_k \equiv \tfrac{1}{2}\mathrm{diag}\left(\boldsymbol{L}_u^k \boldsymbol{C}_k \boldsymbol{L}_w^{k\dagger}\right), \quad \overline{\boldsymbol{w}^2}|_k \equiv \tfrac{1}{2}\mathrm{diag}\left(\boldsymbol{L}_w^k \boldsymbol{C}_k \boldsymbol{L}_w^{k\dagger}\right), \quad \overline{\boldsymbol{v}^2}|_k \equiv \tfrac{1}{2}\mathrm{diag}\left(\boldsymbol{L}_v^k \boldsymbol{C}_k \boldsymbol{L}_v^{k\dagger}\right).
\tag{3.20}
$$

Equation (3.9) and (3.17) comprise the SSST system for the streamwise roll and streak plus turbulence dynamics:

$$
\frac{\mathrm{d}\boldsymbol{C}_k}{\mathrm{d}t} = \boldsymbol{A}_k(\boldsymbol{U})\boldsymbol{C}_k + \boldsymbol{C}_k \boldsymbol{A}_k^{\dagger}(\boldsymbol{U}) + f_k^2 \boldsymbol{Q}_k,
\tag{3.21a}
$$

$$
\frac{\mathrm{d}\boldsymbol{\Gamma}}{\mathrm{d}t} = \boldsymbol{G}(\boldsymbol{\Gamma}) + \sum_k \mathrm{Re}(\boldsymbol{L}_{RS}\boldsymbol{C}_k).
\tag{3.21b}
$$

Equation (3.21a), with dimension $4N_y^2 \times N_z^2$, is a time-dependent Lyapunov equation for the spatial covariance, $\boldsymbol{C}_k$, of the perturbation field at streamwise wavenumber k. This equation involves the perturbation dynamical operator at wavenumber k, $\boldsymbol{A}_k(\boldsymbol{U})$, linearized about the instantaneous streamwise-averaged streamwise flow, $\boldsymbol{U}$. The spatial structure of the parameterized stochastic perturbation forcing is given by $\boldsymbol{Q}_k$ and its amplitude by f_k. Equation (3.21b), with dimension $2N_y \times N_z$, is the evolution equation of the streamwise-averaged flow state, $\boldsymbol{\Gamma}$, which is determined by the dynamical operator of the streamwise-averaged flow $\boldsymbol{G}(\boldsymbol{\Gamma})$ and the perturbation Reynolds stresses

obtained from the sum over all retained k of the perturbation covariances by operating with $\mathbf{L}_{RS}$. This equation is coupled nonlinearly to (3.21a) through the mean flow $\mathbf{U}$.

System (3.21) constitutes a closed, deterministic, autonomous, nonlinear system. Because the SSST system is autonomous, its fixed points

$$\mathbf{A}_k(\mathbf{U}_{eq})\mathbf{C}_{keq} + \mathbf{C}_{keq}\mathbf{A}_k^\dagger(\mathbf{U}_{eq}) = -f_k^2\mathbf{Q}_k, \quad \mathbf{G}(\boldsymbol{\Gamma}_{eq}) = -\sum_k \mathrm{Re}\left(\mathbf{L}_{RS}\mathbf{C}_{keq}\right), \qquad (3.22)$$

identify statistical equilibrium states.

Underlying the SSST dynamics are:

(a) the assumption that perturbation–perturbation interactions and the external sources of turbulence in the perturbation equations can be parameterized as an additive stochastic forcing delta correlated in time;

(b) the ergodic assumption that the streamwise average of the perturbation covariance can be obtained from the ensemble average over realizations of the forcing.

Some of the properties of SSST dynamics are as follows.

(a) SSST constitutes a closure of the streamwise-averaged turbulence dynamics at second-order with the state of the SSST system being the statistical mean state of the turbulence. The SSST system is the dynamics of the co-evolution of the streamwise-averaged flow and a second-order approximation to its associated field of turbulent perturbations. Although the effects of the turbulent Reynolds stresses are retained in this system, the fluctuations of the turbulent Reynolds stresses are suppressed by the ensemble averaging so that the dynamics of turbulence/mean-flow interaction, and particularly the equilibria arising from this interaction, are revealed with great clarity.

(b) The SSST state vector provides a second-order approximation to the probability density function (p.d.f.) of the streamwise-averaged turbulent state. In order to obtain the evolving ensemble mean p.d.f. using direct numerical simulation (DNS) it would be required to perform a number of DNS integrations equal to the state dimension.

(c) The attractor of the SSST system dynamics may be a fixed point, a limit cycle or be chaotic. Examples of each type have been found in the SSST dynamics of geophysical and plasma turbulence (Farrell & Ioannou 2003, 2008a, 2009).

(d) The SSST system introduces a new stability concept: the stability of an equilibrium between a streamwise-averaged flow and its associated field of turbulence. This instability of a SSST equilibrium is called structural and it arises from the mechanism of interaction between the perturbations and the mean flow, which is distinct from the mechanism of hydrodynamic instability.

4. SSST equilibria and their structural stability

Couette flow is an equilibrium of the SSST system at perturbation forcing amplitude $f = 0$. As f increases, new spanwise-independent SSST equilibria are obtained. These equilibria satisfy (3.22) with spanwise-independent $\mathbf{U}_{eq}(y)$ and $\boldsymbol{\Psi}_{eq} = 0$. Consistent with the spanwise independence of both the equilibrium mean flow and the imposed forcing, $\mathbf{C}_{keq}$ is also spanwise independent and it follows that there is no streamwise roll forcing.

We now calculate the change in $\mathbf{C}_{keq}$ resulting from a streak perturbation, $\delta\mathbf{U}_s(y, z)$, to $\mathbf{U}_{eq}(y)$. The streak component, $\mathbf{U}_s$, is here defined as the departure of the streamwise-averaged flow $\mathbf{U}$ from its spanwise average $[\mathbf{U}]$, i.e. $\mathbf{U}_s = \mathbf{U} - [\mathbf{U}]$. With the introduction

of this streak perturbation, C_{keq} no longer satisfies the equilibrium condition, (3.22), and this perturbation results, as seen from (3.21a), in the instantaneous rate of change of the covariance field:

$$\frac{\mathrm{d}C_k}{\mathrm{d}t} = \delta A_k C_{keq} + C_{keq}\delta A_k^\dagger, \tag{4.1}$$

where $\delta A_k = A_k(U_{eq} + \delta U_s) - A_k(U_{eq})$ is the change in the linear operator due to δU_s. This results in a Reynolds stress, which can be obtained from the second component of (3.19), that implies the instantaneous streamwise roll streamfunction acceleration:

$$\partial_{tt}\Psi = \Delta_1^{-1}(-(\partial_{yy} - \partial_{zz})\partial_t\overline{vw} - \partial_{yz}\partial_t(\overline{w^2} - \overline{v^2})), \tag{4.2}$$

where the rates of change of the Reynolds stresses are obtained by introducing the time derivative of C_k into (4.2).

Four example streak perturbations, δU_s, together with vectors of the induced streamwise roll velocity accelerations, $\partial_{tt}(V, W) = \partial_{tt}(-\partial_z\Psi, \partial_y\Psi)$, from (4.2), are shown in figure 3. Remarkably, all of these streak perturbations produce streamwise roll forcing configured to amplify the imposed streak perturbation through the lift-up mechanism. This robust Reynolds stress-mediated feedback between the streamwise streak and roll has important implications for the maintenance of turbulence in shear flows. We will show below that even when the streak structure is highly complex and time dependent, as in a turbulent shear flow, the streamwise roll forcing produced by the perturbation Reynolds stresses remains collocated with the streak so as to amplify the streak. Moreover, this tendency of imposed streaks to induce, through the modification of the perturbation field, streamwise roll forcing with a tendency to reinforce the imposed streak provides the mechanism for a streamwise roll and streak plus turbulence cooperative instability in shear flow. However, most streak perturbations organize turbulent Reynolds stresses that do not exactly amplify the streak that produced them, as is shown prominently in the case of the streak perturbation in figure 3(a). Exponential modal growth of a streak and its associated streamwise roll and perturbation fields results if the streak organizes precisely the perturbation field required for its amplification.

We now show that exponentially unstable streamwise roll and streak modes arise in a spanwise-independent field of forced turbulence if the perturbation forcing amplitude exceeds a threshold. Consider an equilibrium solution (C_{keq}, Γ_{eq}) of (3.22). The stability of this equilibrium is determined by eigenanalysis of the perturbation equations, obtained by taking the first variation of (3.21). These perturbation equations are

$$\frac{\mathrm{d}\delta C_k}{\mathrm{d}t} = A_{keq}\delta C_k + \delta C_k A_{keq}^\dagger + \delta A_k C_{keq} + C_{keq}\delta A_k^\dagger \tag{4.3}$$

$$\frac{\mathrm{d}\delta\Gamma}{\mathrm{d}t} = \sum_i \frac{\partial G}{\partial\Gamma_i}\bigg|_{\Gamma_{eq}}\delta\Gamma_i + \sum_k \mathrm{Re}\left(L_{RS}\delta C_k\right). \tag{4.4}$$

In (4.3), A_{keq} is the linear perturbation operator about the equilibrium mean flow U_{eq}, C_{keq} is the corresponding covariance at equilibrium and $\delta A_k = A_k(U_{eq} + \delta U) - A_k(U_{eq})$ is the change in the linear operator due to δU. The total perturbation to the mean flow is $\delta\Gamma = [\delta U, \delta\Psi]$. The perturbation to the covariance, C_{keq}, is δC_k. Equations (4.3) and (4.4) are linear in δC_k and $\delta\Gamma$ and eigenanalysis of these equations determines the structure and growth rate of the modes of the equilibrium $[C_{keq}, \Gamma_{eq}]$. When the equilibrium, $[C_{keq}, \Gamma_{eq}]$, becomes unstable, the mean flow and the associated perturbation field bifurcate from the equilibrium solution.
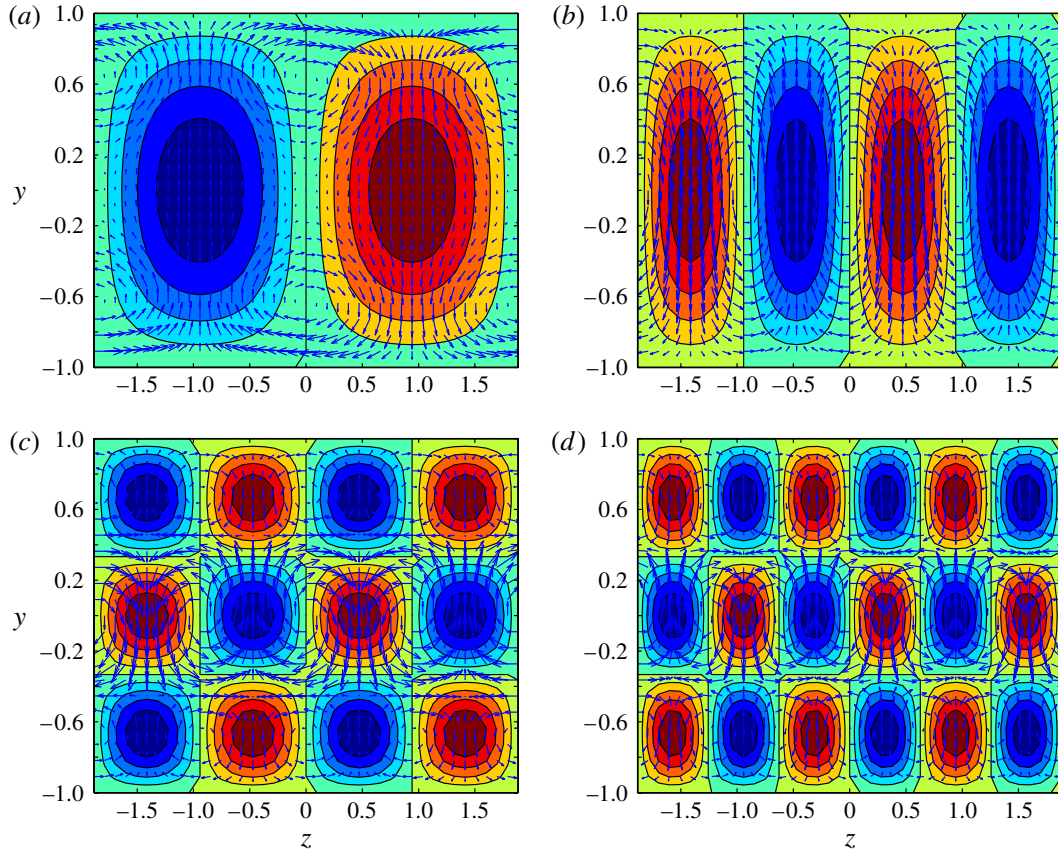
FIGURE 3. (Colour online) The rate of change of streamwise roll acceleration induced by streak perturbations to a Couette flow that is maintained turbulent by stochastic forcing. Distortion of the turbulence by the streak perturbation induces Reynolds stresses that force roll circulations supporting the streak via the lift-up mechanism. Shown are contours of the imposed streak perturbations, δU, and vectors of the resulting rate of change of roll acceleration, $(\ddot{V}, \ddot{W})$. This figure demonstrates the tendency for streamwise streak perturbations to organize supporting streamwise-averaged roll forcing from the perturbation field. The Reynolds number is $R = 400$, the perturbation forcing amplitude is $f = 4.1$, the spanwise width is $L_z = 1.2\pi$ and the streamwise wavenumber is $k = 2\pi/(1.75\pi) = 1.143$: (*a*) $\delta U = \cos(\pi y/2) \sin(2\pi z/L_z)$; (*b*) $\delta U = \cos(\pi y/2) \sin(4\pi z/L_z)$; (*c*) $\delta U = \cos(3\pi y/2) \sin(4\pi z/L_z)$; (*d*) $\delta U = \cos(3\pi y/2) \sin(6\pi z/L_z)$.

For sufficiently high turbulence intensities, the spanwise-independent equilibria become structurally unstable with exponentially growing mean flow eigenfunctions in the form of streamwise rolls and streaks. We demonstrate this for a channel with $L_z = 1.2\pi$, at $R = 400$, and for a perturbation field at the single streamwise wavenumber $k = 1.143$. This channel geometry is the same as that used in most of the simulations of Hamilton *et al.* (1995). The power method is used to find the structure and growth rate, λ, of the most unstable eigenmode of equations (4.3) and (4.4). The calculations use $N_y = 21$ and $N_z = 40$ points, with convergence verified at double resolution.

The spanwise-independent equilibrium is stable for $f \leqslant f_c = 4.75$, with f the perturbation forcing amplitude at the retained wavenumber. At f_c this equilibrium becomes structurally unstable, while remaining hydrodynamically stable. The most
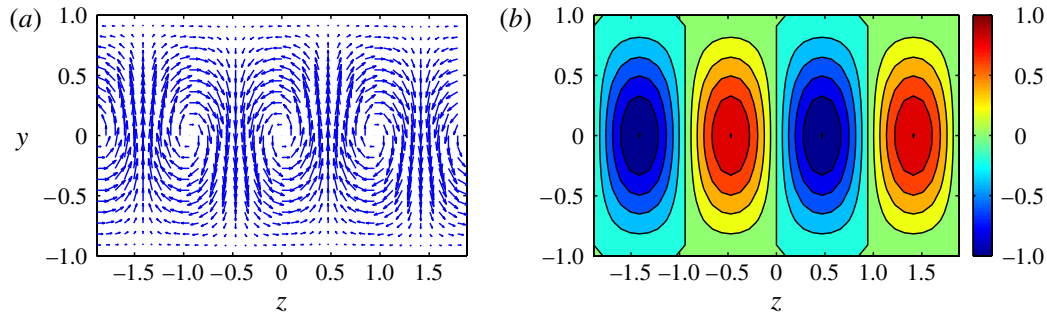
FIGURE 4. (Colour online) The most unstable streamwise roll and streak eigenfunction of the SSST system linearized about the spanwise uniform equilibrium at perturbation forcing amplitude $f = 6.86$. The growth rate of this mode is $\lambda = 0.014$. Shown are velocity vectors $(\delta V, \delta W)$ (*a*) and streamwise velocity δU (*b*). The maxima of $(\delta U, \delta V, \delta W)$ are proportional to $(1, 0.06, 0.03)$. Consistent with the lift-up mechanism, positive δV is associated with negative δU. This figure demonstrates that the tendency for streamwise streak perturbations to organize supporting streamwise roll forcing from the forced turbulence, shown in figure 3, leads to the formation of an unstable streamwise roll and streak eigenmode. Other parameters are as in figure 3.
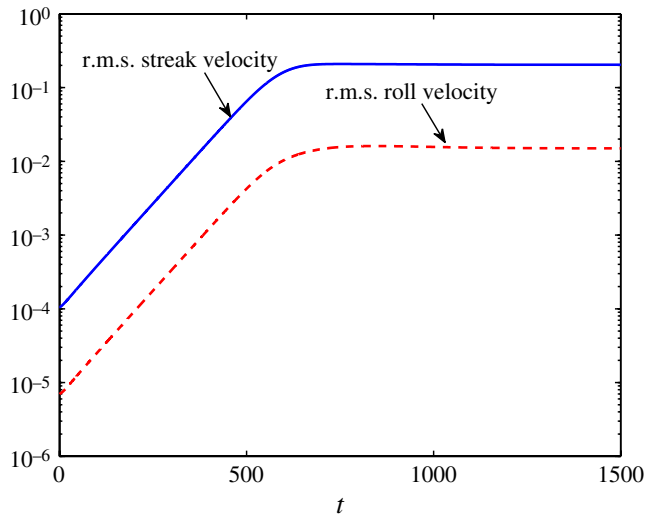
FIGURE 5. (Colour online) Growth and equilibration of the streamwise roll and streak eigenfunction shown in figure 4. The r.m.s. streak velocity and r.m.s. roll velocity initially grow exponentially with the predicted growth rate, $\lambda = 0.014$, until $t \approx 600$ after which an equilibrium is established. This figure demonstrates that SSST dynamics includes the nonlinear mechanism of streak equilibration as well as the mechanism of unstable streamwise roll and streak growth.

unstable eigenfunction at $f = 6.86$ is shown in figure 4. When this eigenfunction is introduced into the SSST system with small amplitude, it grows at first exponentially at the rate predicted by its instability and then asymptotically equilibrates at finite amplitude, as shown in figure 5. This equilibrium solution, shown in figure 6, is a steady, finite-amplitude streamwise roll and streak.
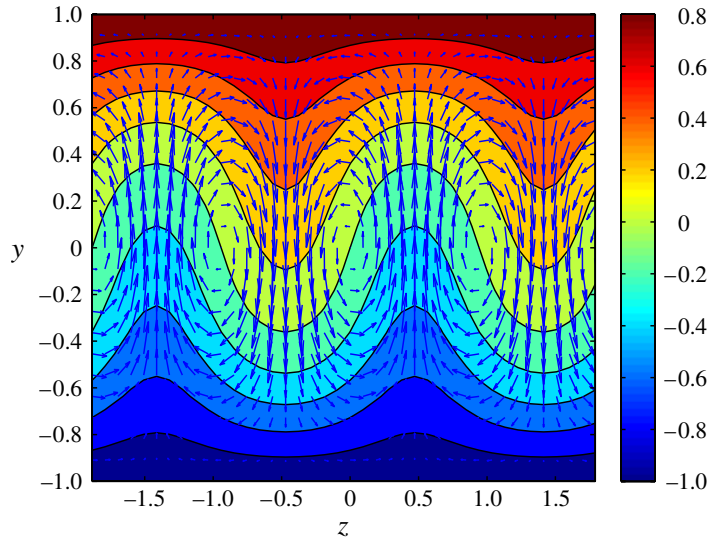
FIGURE 6. (Colour online) The finite-amplitude streamwise roll and streak resulting from the equilibration of the eigenmode shown in figure 4. Shown are the streamwise-averaged streamwise flow, $U(y, z)$, (contours) and the streamwise-averaged velocities, (V, W) (vectors). Consistent with the lift-up mechanism, positive V is associated with a decrease in U. The maxima of the fields (U, V, W) are $(0.26, 0.02, 0.009)$. The perturbation forcing amplitude for this equilibrium is $f = 6.86$.

The bifurcation diagram of the SSST equilibria is shown in figure 7 as a function of bifurcation parameter f. The finite-amplitude streamwise roll and streak equilibria are structurally stable for $f_c \leqslant f \leqslant f_u$. At $f_u = 6.9$ there is a second bifurcation in which the equilibrium becomes structurally unstable, while remaining hydrodynamically stable. Examples of these equilibria are shown in figure 8. In these equilibria the spanwise average flow profile, $[U]$, departs only slightly from the Couette flow profile, $U = y$. Indicative of this nearness to Couette flow is the low viscous dissipation rate of the flow in these equilibria. This dissipation rate is defined as

$$D = \frac{1}{R} \frac{1}{2L_x L_y L_z} \int_0^{L_x} \int_{-L_y}^{L_y} \int_0^{L_z} |\boldsymbol{\omega}|^2 \, \mathrm{d}x \, \mathrm{d}y \, \mathrm{d}z \tag{4.5}$$

where $\boldsymbol{\omega} = \nabla \times \boldsymbol{u}$ is the total vorticity of the flow. The minimum dissipation rate, D_C, is obtained for Couette flow and the ratio, D/D_C, for equilibria with $f_c \leqslant f \leqslant f_u$ is in the range $1 \leqslant D/D_C < 1.4$, while this ratio is of order three in the turbulent state.

The nearly laminar streamwise roll and streak equilibria shown in figure 8 have spanwise wavenumber 2. For the equilibrium at $f = 6.86$, this wavenumber corresponds to a streak spacing, expressed in wall units, of $z^+ = 45$. The non-dimensional wall unit, which is indicated by a superscript $+$, is defined as $l_\nu \equiv (R[U_y(-1)])^{-1/2}$, where $[U_y(-1)]$ is the spanwise-averaged shear at the lower boundary. We note that this streak spacing is about half the $z^+ = 100$ seen in turbulent boundary layers (Smith & Metzler 1983). As we show below, when the SSST system transitions to the time-dependent state the streak spacing becomes $z^+ = 100$, as observed in turbulent flows.

Analogous bifurcation behaviour is obtained if the Reynolds number is used as the bifurcation parameter instead of the perturbation forcing amplitude. A regime diagram
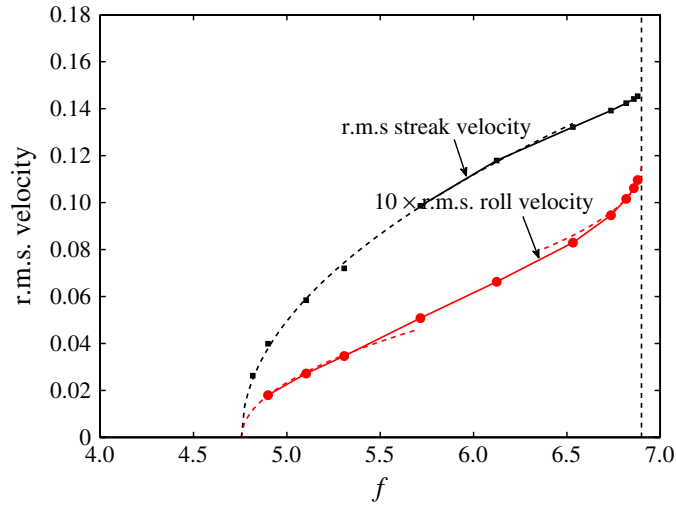
FIGURE 7. (Colour online) SSST bifurcation diagram for the Couette problem. Shown are the r.m.s. streak velocity (squares) and r.m.s. streamwise roll velocity (circles) as a function of the perturbation forcing amplitude, f. For $f < 4.75$, both the streamwise streak and roll velocities are zero. At $f_c = 4.75$ the spanwise uniform equilibrium bifurcates to an equilibrium with a streamwise roll and streak. The dashed line indicates the $\sqrt{f - f_c}$ dependence of the streamwise roll and streak velocities near this critical f_c. Stable streamwise roll and streak equilibria extend up to $f_u = 6.9$ beyond which the streamwise roll and streak transitions to a time-dependent state. The dashed line indicates the $\sqrt{f_u - f}$ dependence of the streamwise roll and streak amplitude near this critical f_u. The Reynolds number is $R = 400$, the spanwise width is $L_z = 1.2\pi$ and the streamwise wavenumber is $k = 2\pi/(1.75\pi) = 1.143$.

showing the bifurcation boundaries as a function of both R and f is shown in figure 9. Bifurcation from spanwise uniform equilibria to stable equilibria with streamwise rolls and streaks occurs on crossing the curve indicated $f_c(R)$, and bifurcation to a time-dependent state occurs on crossing $f_u(R)$. From figure 9, it is clear that the threshold curve, $f_u(R)$, for transition to the time-dependent state is very accurately fit by the function: $f_u(R) = 2200/(R - 89)$. This function suggests that the turbulence intensity, $\{I_u\}$, producing structural instability scales asymptotically as $R^{-\alpha}$ with $\alpha = 1$. Bifurcation to this time-dependent state implies transition to turbulence in the SSST system and therefore α provides a Reynolds number scaling for the threshold value of f producing transition to turbulence for sufficiently small initial conditions. The same, or nearly the same, exponent is obtained by assuming that transition is determined by the Reynolds number scaling of the amplitude of an initial condition required to produce a marginally hydrodynamically unstable streamwise streak (Kreiss, Lundbladh & Henningson 1994; Reddy *et al.* 1998; Chapman 2002).

   In laboratory experiments or DNS simulations of forced turbulence there is likely to be a finite-amplitude optimal or near-optimal initial condition at least episodically present in the turbulence that would serve to initiate the growth of a streamwise roll and streamwise streak and set the streak spacing in the spanwise direction (Brandt *et al.* 2002). When initiated by a sufficiently small streamwise roll perturbation, the perturbation/mean-flow interaction would result in an increase in growth rate of the evolving transient streamwise roll and streak for subcritical turbulence intensity, corresponding to $f < f_c$. This increase in growth rate would be followed by finite amplitude equilibration for higher turbulence intensities in the range $f_c \leqslant f \leqslant f_u$,
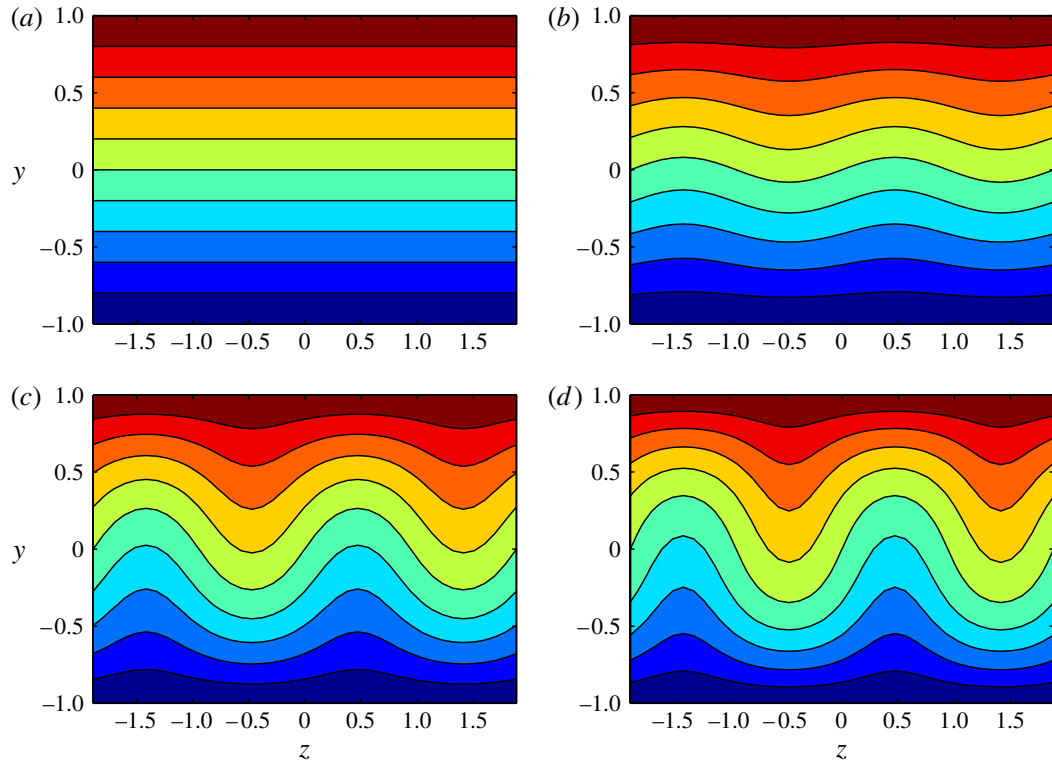
FIGURE 8. (Colour online) Streamwise-averaged velocity of the SSST equilibria in figure 7 at various values of f. (a) The equilibrium at $f = 4.1$ is spanwise uniform. (b) At $f = 4.9$ the spanwise uniform flow is structurally unstable and leads to an equilibrium with a weak streak. (c) The equilibrium at $f = 6.1$. (d) The equilibrium at $f = 6.86$. The streamwise-averaged flow associated with these equilibria becomes increasingly inflected in the cross-stream as $f \to f_u$. The contour interval is 0.2.

and by transition to time dependence for $f > f_u$. For example, consider an initial condition consisting of the $t = 50$ optimal among streamwise roll perturbations. When this perturbation is introduced into a Couette flow at $R = 400$ in the presence of turbulence with various values of f the resulting evolution is as shown in figure 10. The optimal initial condition is seen to recruit the turbulent perturbation field to support and maintain itself, producing increased growth for $f \leqslant f_c$; increased growth followed by approach to a finite-amplitude equilibrium for $f_c \leqslant f \leqslant f_u$; and, ultimately, destabilization for $f > f_u$. These examples demonstrate how a sufficiently small-amplitude optimal initial streamwise roll structure is effectively converted into a SSST eigenmode in the presence of a forced turbulence field. This eigenmode then promotes transition to a time-dependent state. However, as the amplitude of the initial streamwise roll perturbation increases, the transient growth mechanism would increasingly dominate the streamwise roll and streak growth process.

5. Dynamics of the SSST streamwise roll and streak in Couette flow

Diagnostics of the dynamics of the streamwise roll and streak are shown in figure 11. The streamwise roll is maintained solely by the perturbation Reynolds stress (cf. figure 11c) while the streamwise streak is maintained by the lift-up mechanism (cf. Figure 11b). The direct effect of the Reynolds stress on the streamwise streak is to damp it (cf. figure 11d).
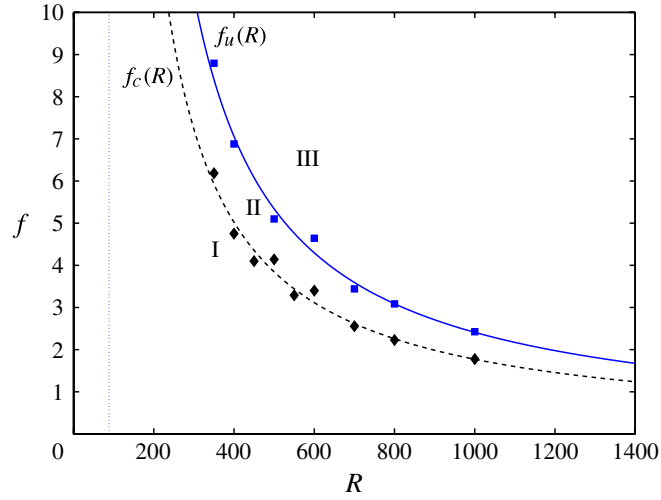
FIGURE 9. (Colour online) SSST streamwise roll and streak regime diagram for the Couette problem. In region I the equilibria are spanwise uniform. In region II the equilibria are streamwise roll and streaks. In region III there are no equilibria and only time-dependent streamwise roll and streak structures exist. The curves $f_c(R)$ (squares) and $f_u(R)$ (triangles) indicate structural instability boundaries. The instability boundary for transition to the time-dependent state is well fit by the function $f_u = 2200/(R - 89)$ (solid). This figure implies that either R or f could be used as the bifurcation parameter in the SSST dynamics and that the associated volume-averaged turbulence intensity, $\{I_u\}$, required to assure transition to the time-dependent state in SSST dynamics decreases asymptotically as R^{-1}. The spanwise width is $L_z = 1.2\pi$ and the streamwise wavenumber is $k = 2\pi/(1.75\pi) = 1.143$.

We turn next to examine the structure of the perturbation field associated with the streamwise roll and streak equilibrium, making use of the proper orthogonal decomposition (POD) method (Lumley 1967). In the POD method the perturbation field structures are ordered according to their contribution to the total perturbation energy. This is achieved by performing an eigenanalysis of $\boldsymbol{M}_k^{1/2}\boldsymbol{C}_{keq}\boldsymbol{M}_k^{1/2}$, where $\boldsymbol{C}_{keq}$ is the equilibrium covariance and $\boldsymbol{M}_k$ is the energy metric (3.12) (cf. Farrell & Ioannou 1993e). The result is a complete set of eigenfunctions that are orthogonal in energy, called empirical eigenfunctions (EEs). We find that the perturbation energy is spread over many of these EE structures, but as f increases, a single EE becomes dominant and its structure becomes an increasingly good representation of the perturbation field. For the equilibrium at $f = 6.86$, the dominant EE, which accounts for 24 % of the perturbation energy, is shown in figure 12. This EE is a sinuous oblique structure collocated with the streak. Its structure is very close to that of the least damped mode of $\boldsymbol{A}_k(\boldsymbol{U}_{eq}(y, z))$. The eigenvalues, σ, of $\boldsymbol{A}_k(\boldsymbol{U}_{eq})$, are shown in figure 15 for the equilibria of figure 8. The emergence of this sinuous mode, which has been implicated in streak breakdown and transition to turbulence, is apparent (Kim *et al.* 1971; Jiménez & Moin 1991; Hamilton *et al.* 1995; Waleffe 1997; Reddy *et al.* 1998).

This dominance of the sinuous mode in the perturbation field need not result from unstable mode growth. In fact, as was noted by Schoppa & Hussain (2002), this mode emerged in their simulations primarily from non-normal growth processes. In Appendix we show how the optimal perturbation for exciting this sinuous mode is calculated and in figure 13 we show this optimal perturbation. Owing to the high non-normality of $\boldsymbol{A}_k(\boldsymbol{U}_{eq}(y, z))$, introduction of the perturbation that optimally excites

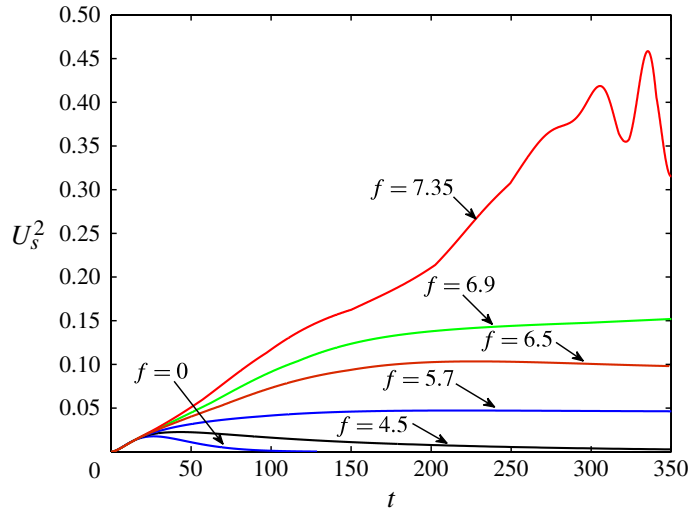*B. F. Farrell and P. J. Ioannou*

FIGURE 10. (Colour online) Development of a streamwise roll and streak initial condition in the presence of various perturbation forcing amplitudes in Couette flow as indicated by the maximum square streak velocity, U_s^2. The initial condition is the $t = 50$ optimal among perturbations with $k = 0$ excited with r.m.s. velocity amplitude 0.05 % of the maximum velocity of the Couette flow, U_0. The optimal is evolved in the presence of forced turbulence in equilibrium with perturbation forcing amplitudes; $f = 0$, 4.5, 5.7, 6.5, 6.9, 7.35. The curve for $f = 0$ indicates the transient growth followed by decay of this initial perturbation in the absence of feedback from the forced turbulence. Note that for $f < f_c = 4.75$ the streak initially grows but then decays, with the rate of decay reduced by its interaction with the forced turbulence. For $f_c < f < f_u = 6.9$, the optimal evolves to a non-decaying streamwise roll and streak equilibrium structure, while for $f > f_u$, it becomes structurally unstable and ultimately time dependent. This figure shows that interaction with turbulence sustains the growth of an optimal initial condition. The Reynolds number is $R = 400$, the spanwise width is $L_z = 1.2\pi$ and the streamwise wavenumber is $k = 2\pi/(1.75\pi) = 1.143$.

the sinuous mode results in energy growth by a factor of 1900 more than would introduction of the mode itself. While the optimal perturbation for exciting the mode is the optimal perturbation in the limit of large time, the perturbation that results in optimal growth over 10 units of time has similar structure and produces comparable growth, as shown in figure 14. For understanding the RGP it is important to note that coherent forcing of the streamwise rolls results from both the optimal for exciting the mode and the optimals over shorter times (cf. Figure 14).

The sinuous mode produces Reynolds stresses that force the streamwise roll, and thereby indirectly force the streak, but also produces Reynolds stress that directly damp the streak. This dual role of the sinuous mode in both forcing and damping the streak is explicitly modelled in the fourth-order system of Waleffe (1997) (cf. his equation (20)).

To compare the relative contributions of the Reynolds stress arising from the sinuous mode in damping the streak to the indirect effect of its Reynolds stress in building the streak, via its forcing of the streamwise roll, we impose a modification of the real part of the eigenvalue of the mode at equilibrium. Specifically, if σ_{rE} is the damping rate of the sinuous mode, we set this damping rate equal to $0.9\sigma_{rE}$ (less damped) and $1.1\sigma_{rE}$ (more damped), and advance the SSST (3.21) in time. When the mode is more damped, the streak amplitude increases while when the mode is less damped, the
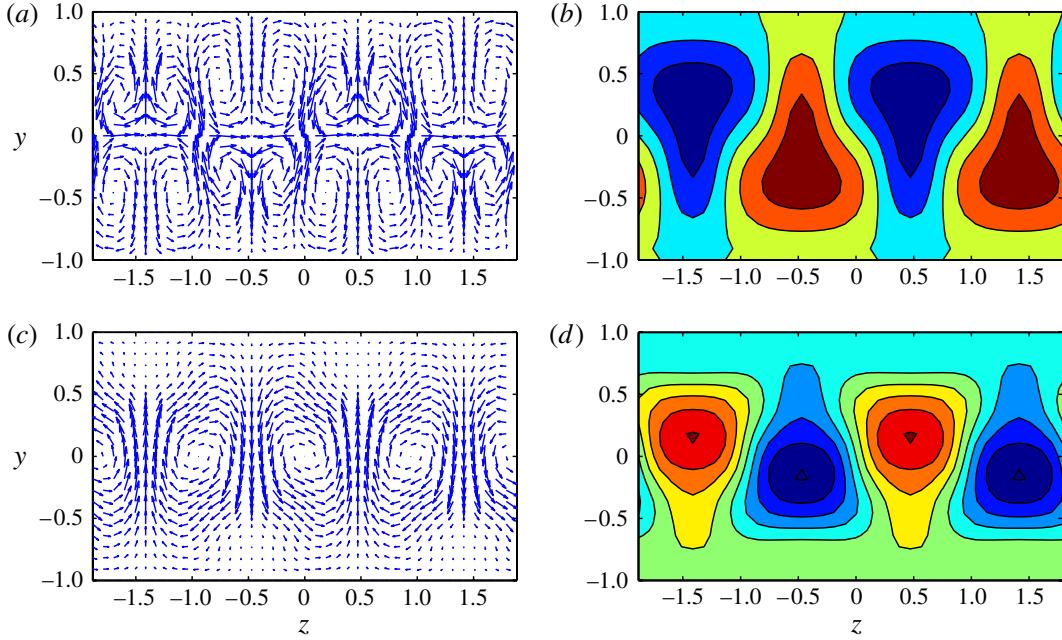
FIGURE 11. (Colour online) Diagnostics of the dynamics of the streamwise roll and streak SSST equilibrium shown in figure 6. (*a*) Acceleration of the streamwise roll, $(\dot{V}, \dot{W})$, resulting from self-advection by the mean roll velocity, (V, W). The maximum of $\dot{V}$ is 10^{-4}. (*b*) Acceleration of the streamwise-averaged streamwise flow, $\dot{U}$, induced by the streamwise roll, the maximum of $\dot{U}$ is 10^{-2}, mainly due to the lift-up mechanism, $(-U_y V)$. (*c*) Acceleration of the streamwise roll, $(\dot{V}, \dot{W})$, resulting from the perturbation Reynolds stresses. The maximum of $\dot{V}$ is 10^{-3}. This term exceeds the self-advection by the streamwise roll velocities, shown in (*a*), by an order of magnitude and determines the structure of the streamwise roll. (*d*) Acceleration of the streamwise-averaged streamwise flow, $\dot{U}$, induced directly by the perturbation field Reynolds stresses. This term has maximum magnitude 10^{-2} and decelerates the streak. This figure demonstrates that the finite-amplitude streamwise roll and streak is maintained indirectly by the perturbation driven streamwise roll, through the lift-up mechanism, while the direct effect of the perturbation Reynolds stress is comparable in magnitude and configured to decelerate the streak: (*a*) $\text{curl}(\Delta^{-1}((VW)_{zz} - (VW)_{yy} - (W^2)_{yz} + (V^2)_{yz})i)$; (*b*) $-U_y V - U_z W$; (*c*) $\text{curl}(\Delta^{-1}(\langle vw \rangle_{zz} - \langle vw \rangle_{yy} - \langle w^2 \rangle_{yz} + \langle v^2 \rangle_{yz})i)$; (*d*) $-\langle uv \rangle_y - \langle uw \rangle_z$.

streak amplitude decreases, as shown in figure 16. We conclude that the net effect of the sinuous mode is to stabilize this equilibrium streak.

The perturbation field is supported by transient growth, primarily of the optimal perturbations. Moreover, these optimal perturbations also provide the coherent vorticity forcing maintaining the streamwise rolls. Although this tendency to generate streamwise vorticity occurs regardless of the presence of the streak (cf. figure 14 case with $f = 4.1$), the streak collocates these optimal evolving structures, aligning them so that their Reynolds stress divergence coherently forces the streamwise roll.

6. SSST analysis of streamwise roll and streak growth in the Blasius boundary layer under the parallel flow approximation

While Couette flow is a canonical problem for theoretical study, many of the simulations and observations available for comparison with theory for the
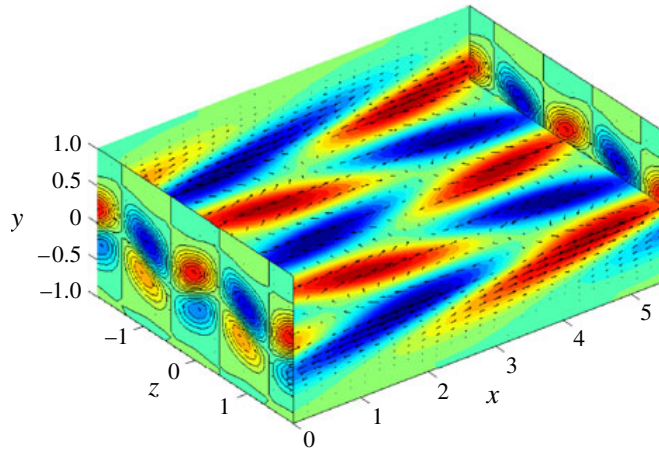
FIGURE 12. (Colour online) Velocity field of the first energy POD EE for the equilibrium with $f = 6.86$, shown in figure 6. This EE alone accounts for 24 % of the perturbation energy. Velocity vectors are superposed on contours of streamwise velocity, which has maximum $u = 0.16$. This figure demonstrates that a dominant sinuous wave structure, collocated with the streak, arises from the interaction between the streak and the forced turbulence field.
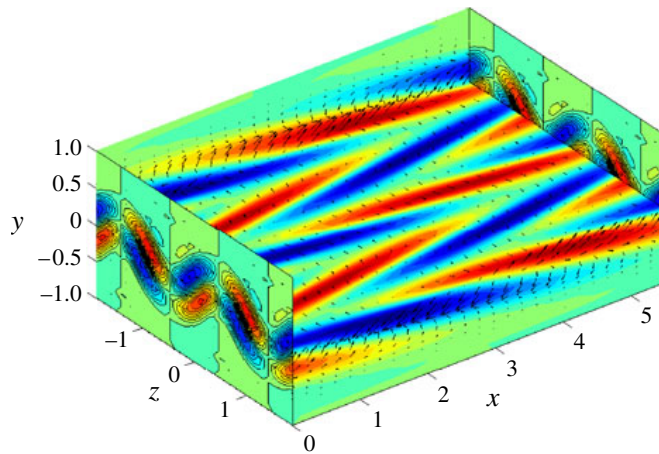

FIGURE 13. (Colour online) Velocity field of the perturbation that optimally excites the least-damped sinuous mode, which has structure very close to the EE shown in figure 12. Optimal perturbations that maximize energy amplification for shorter time periods have similar structure. A unit energy initial condition in the form of this perturbation excites the sinuous mode in energy by a factor of 1900 greater than an initial condition consisting of the sinuous mode itself. It follows that the sinuous mode amplitude, and by extension the first EE of the POD, arises from perturbations in the forced turbulence almost entirely due to non-normal growth processes.

emergence of streamwise rolls and streaks involve boundary layer flows, particularly developing Blasius flow. Computational resource limitations prevent us from solving the developing flat plate boundary layer problem. Instead, we have chosen to study a Blasius boundary layer profile that is maintained constant in the streamwise direction. This parallel flow approximation is widely applied in relating non-normal growth and
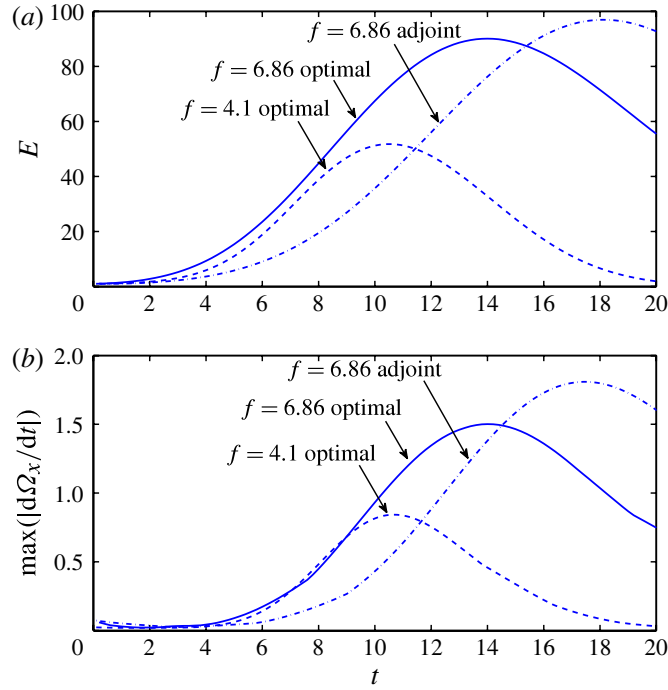
FIGURE 14. (Colour online) Energy growth and associated streamwise roll forcing resulting from energy optimal perturbations to equilibria with Couette boundary forcing. (*a*) Energy growth of the $t = 10$ optimal perturbation to the streak equilibrium at $f = 6.86$ (solid), and to the spanwise uniform equilibrium at $f = 4.1$ (dashed) (respectively shown in figure 8*d,a*). The optimal is excited at unit energy and has streamwise wavenumber $k = 1.143$. Also shown is the growth of the adjoint mode which excites optimally the least-damped mode of $\boldsymbol{A}_k(\boldsymbol{U}_{eq})$ for the equilibrium flow at $f = 6.86$ (dash-dot). (*b*) Associated streamwise roll forcing induced by these optimal perturbations as indicated by the maximum rate of change of streamwise vorticity, $|\dot{\Omega}_x|$. This figure demonstrates that streamwise roll forcing is associated with optimal growth and that optimal perturbations produce streamwise roll forcing regardless of the presence of a streak. The streak serves only to collocate the streamwise roll forcing.

modal instability analyses to observations and simulations of developing boundary layers (Schlatter *et al.* 2008; Cossu *et al.* 2011).

Consider a Blasius boundary layer flow, $U_{bl}(y)$ (cf. Batchelor 2000, p. 310), in which the parallel flow assumption has been made so that the flow is maintained as a stationary solution at a chosen fixed Reynolds number. The Reynolds number is defined as $R_{\delta*} = U_\infty \delta^*/\nu$, with U_∞ the free stream velocity, ν the kinematic viscosity, $\delta^* \equiv 1.72\delta$ the displacement thickness and δ the Blasius length scale, $\delta = \sqrt{\nu l/U_\infty}$, in which l is the distance from the leading edge. The channel size is $L_y = 7$ and $L_z = 2\pi/m$, where m is the spanwise wavenumber of the streamwise roll and streak under study. A discretization on $N_y = 30$, $N_z = 30$ grid points is used. The stochastic forcing is limited to a single streamwise wavenumber, $k = m$. The stochastic forcing covariance matrix, $\boldsymbol{Q}_k$, given in (3.11), has been scaled so that perturbation forcing amplitude f maintains at equilibrium the percentage volume-averaged turbulence intensity $\{I_u\} = f/\sqrt{3}$, when the Blasius flow is forced with this scaled $\boldsymbol{Q}_k$. The Blasius profile is maintained in SSST equilibrium for chosen values of the perturbation forcing amplitude, f, by introducing the necessary body force in the streamwise direction into (3.21*b*).
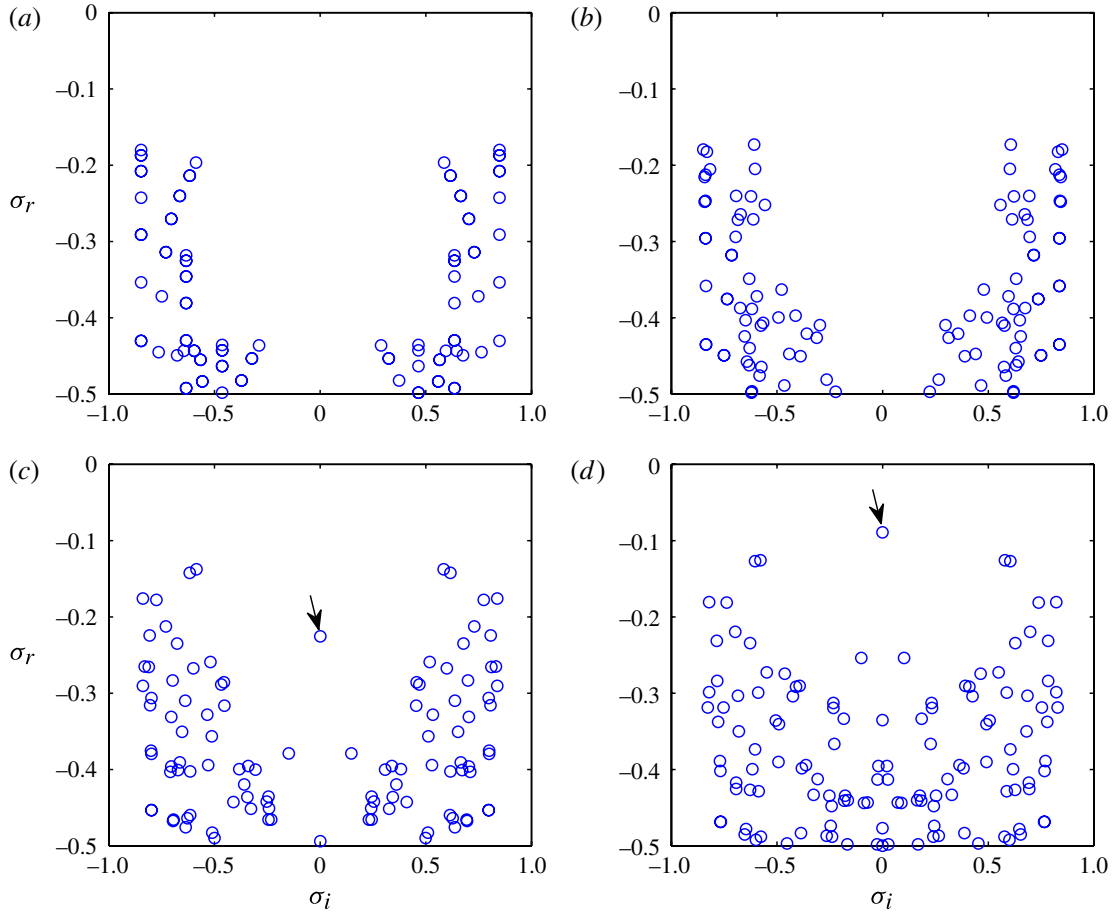
FIGURE 15. (Colour online) Emergence of the sinuous mode of the equilibria in figure 8. Shown are the least-stable eigenvalues, (σ_r, σ_i), of the operator, $\mathbf{A}_k$. Note the emergence of the prominent mode as the streak increases in magnitude with increasing f (arrow). This is the sinuous mode that is commonly observed to accompany streaks nearing transition to turbulence: $(a) f = 4.1$; $(b) f = 4.9$; $(c) f = 6.1$; $(d) f = 6.86$.

The most unstable SSST streamwise roll and streak eigenmode and its growth rate is obtained from (4.4) for $R_{\delta*} = 600$ and $R_{\delta*} = 1200$ by using the power method. For the perturbation forcing amplitude $f = 1.5$, this growth rate as a function of m is shown in figure 17(c). At $R_{\delta*} = 600$ the maximum growth rate occurs at $m_{max} = 1.2$ while at $R_{\delta*} = 1200$ the wavenumber of the maximum moves to $m_{max} = 2.3$. These spanwise wavenumbers correspond to spacing between low-speed streaks of $\Delta z = 3\delta^*$ for $R_{\delta*} = 600$ and $\Delta z = 1.6\delta^*$ for $R_{\delta*} = 1200$, which contrasts with streak spacings between $4\delta^*$ and $7\delta^*$ seen in developing Blasius boundary layers (Westin *et al.* 1994; Matsubara & Alfredsson 2001). This discrepancy can be explained by noting that the initial condition for the instability is provided by the optimal, which sets the spanwise scale of the streamwise roll and streak, with its subsequent growth augmented by the SSST instability. A related linear/nonlinear two-stage growth process was studied previously by Berlin & Henningson (1999) and Brandt *et al.* (2002).

The global optimal occurs at $m_{opt} = 0.51$ with optimal energy growth $G_{opt} = 1681$ at $R_\delta^* = 1200$ and $G_{opt} = 400$ at $R_\delta^* = 600$, as shown in figure 17(a). This spanwise
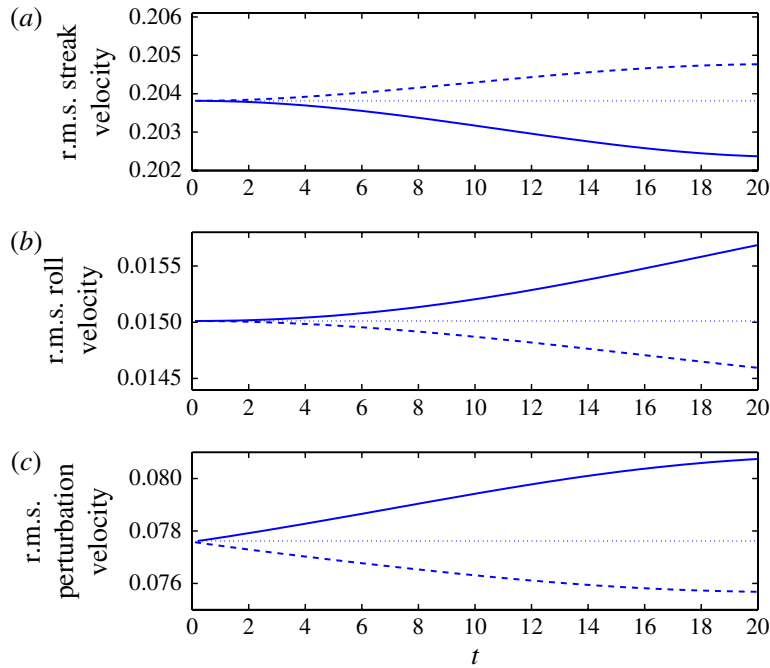
FIGURE 16. (Colour online) Influence of damping the sinuous mode on equilibrium streak amplitude. Shown as a function of time for both increase and decrease in sinuous mode damping are: r.m.s. streak amplitude (*a*), r.m.s. roll amplitude (*b*), and r.m.s. perturbation velocity (*c*), for decreasing (solid) and increasing (dashed) the damping rate of the sinuous mode compared with its damping rate at equilibrium. The corresponding values at equilibrium are also shown (dotted). The equilibrium is that at $f = 6.86$, shown in figure 6. Although the sinuous mode both drives and damps the streak, this figure demonstrates that the net effect of the sinuous mode is to damp the streak.

wavenumber, m_{opt}, corresponds to streak spacing $\Delta z = 7.2\delta^*$. Similar results were obtained by Butler & Farrell (1992) under the parallel flow assumption and in spatially developing Blasius boundary layers by Andersson *et al.* (1999) and Luchini (2000). The structure of the streak at t_{opt}, shown in figure 17(*b,c*), also agrees with these previous results and the SSST unstable mode at m_{opt} has this same streak structure (cf. figure 17*e*,*f*). Notably, and in contrast to the decay with time of the amplitude of the optimal streamwise roll, the streamwise roll associated with this SSST mode continues to grow in amplitude in time as shown in figure 18 for the case of Blasius flow maintained at $R_{\delta*} = 1200$ with perturbation forcing amplitude $f = 1.25$. This increase of the amplitude of the streamwise roll with time agrees with the observations of Alfredsson & Matsubara (1996).

We now show that with perturbation forcing amplitude $0 < f < f_u$, with f_u the threshold amplitude for structural instability, a streamwise roll of sufficiently small initial amplitude attains greater growth than it would in the absence of turbulence, but ultimately decays, while for $f > f_u$, even a small-amplitude initial condition eventually evolves into an exponentially growing structure (we did not find any stable streamwise roll and streak equilibria in Blasius flow). Development of the global optimal in the presence of four levels of perturbation forcing amplitude is shown in figure 19 for the case of a Blasius flow maintained at $R_{\delta*} = 1200$. Augmentation of the optimal growth (cf. the curve for $f = 0$) by interaction with the perturbations is clear (cf. the
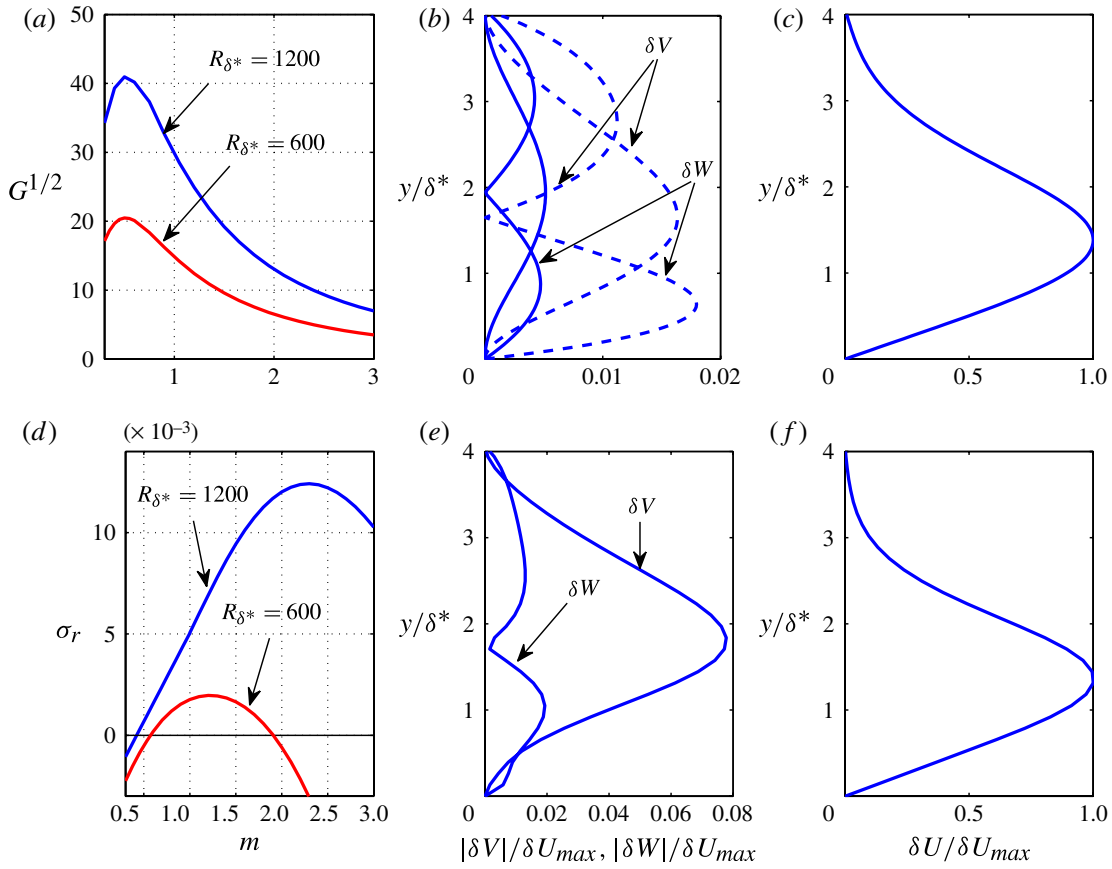
FIGURE 17. (Colour online) SSST streamwise roll and streak eigenmode growth and optimal growth in a Blasius boundary layer at Reynolds numbers $R_{\delta*} = 600$ and $R_{\delta*} = 1200$. (*a*) Square root of the optimal energy growth factor, $\sqrt{G}$, of $k = 0$ perturbations as a function of spanwise wavenumber of the streak, m. The global optimal growth, $G = 1681$, for $R_{\delta*} = 1200$, occurs at spanwise wavenumber $m_{opt} = 0.51$, which corresponds to streak spacing $\Delta z = 7.2\delta^*$. The time at which this optimal growth occurs is $t_{opt} = 960$. (*b*) Streamwise roll velocities, $(\delta V, \delta W)$, of the global optimal for $R_{\delta*} = 1200$, at $t = 0$ (dash) and t_{opt} (solid). (*c*) Streak velocity, δU, of the global optimal for $R_{\delta*} = 1200$ at t_{opt}. (*d*) SSST eigenmode growth rate as a function of the eigenmode spanwise wavenumber, m, for perturbation forcing amplitude $f = 1.5$. Perturbation streamwise wavenumbers are chosen so that $k = m$. The maximum growth rate for $R_{\delta*} = 1200$ is $\sigma_r = 0.0125$ and occurs at spanwise wavenumber $m = 2.3$. The maximum growth rate for $R_{\delta*} = 600$ is $\sigma_r = 0.002$ and occurs at $m = 1.2$. (*e*) Streamwise roll velocities, $(\delta V, \delta W)$ and (*f*) streak velocity, of the unstable mode at m_{opt} and $R_{\delta*} = 1200$. The growth rate at m_{opt} is $\sigma_r = 0.001$. This figure demonstrates that the optimal perturbation and the SSST unstable mode coexist and that the structure of the optimal perturbation is nearly identical to that of the unstable eigenmode at m_{opt}.

curve for $f = 0.5$). For a streamwise roll with spanwise wavenumber m_{opt} the structural instability threshold is at $f_u = 0.8$, and for any $f > f_u$ the flow eventually transitions to the time-dependent state regardless of the amplitude of the initial perturbation. This transition to a time-dependent state is shown in figure 19 for $f = 1.25$ and $f = 1.5$. Experiments in developing boundary layers reported in Andersson *et al.* (1999) show that for the Reynolds number $Re_T = 486\,750$, equivalent to $R_\delta^* = 1200$, transition occurs at $Tu \approx 1.8\,\%$. The value $f_u = 0.8$, equivalent to $\{I_u\} = 0.46\,\%$, is predicted for transition for arbitrarily small initial roll perturbations by our parallel flow model. The
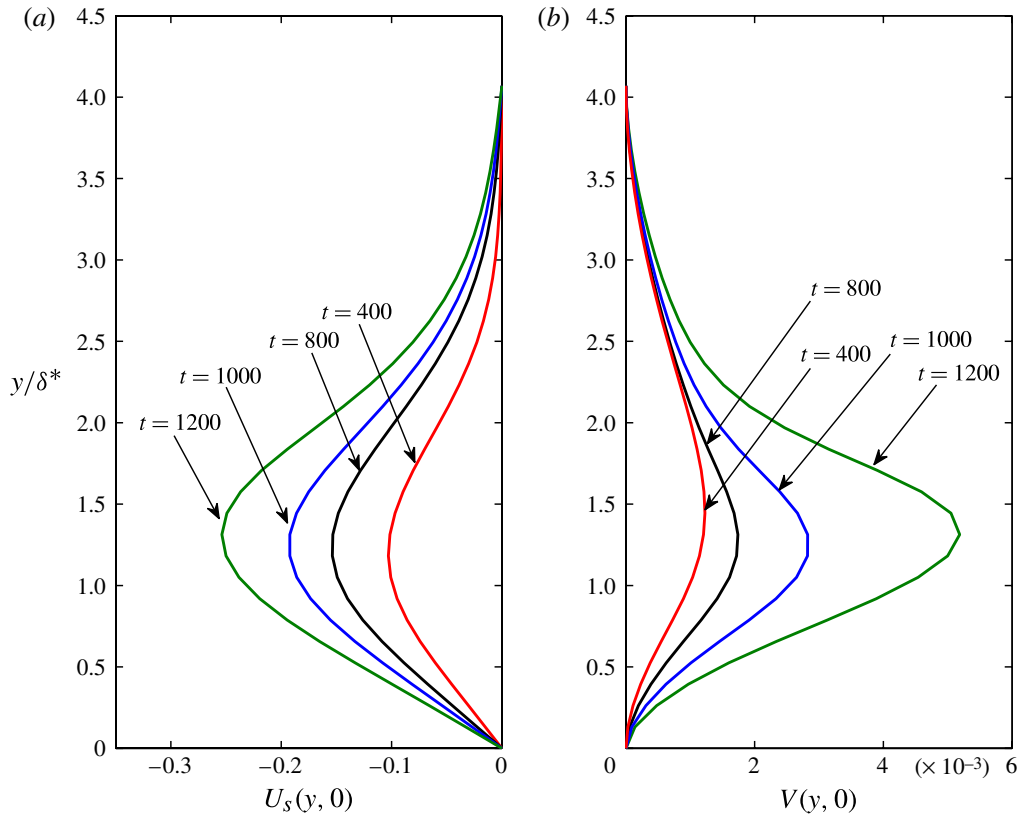
FIGURE 18. (Colour online) Effect of turbulence on the development of the global optimal structure in Blasius flow at $R_{\delta*} = 1200$. The global optimal perturbation at $m_{opt} = 0.51$ (cf. figure 17b,c) is excited at r.m.s. velocity 0.1 % of the free stream velocity, U_∞, in the presence of turbulence with $f = 1.25$ at perturbation streamwise wavenumber $k = 0.51$. Shown are the low-speed streak velocity (a) and the cross-stream component of the streamwise roll velocity, V (b) at $t = 400, 800, 1000, 1200$, all prior to transition. The figure shows that in the presence of forced turbulence the cross-stream velocity increases together with the streak. In contrast, for $f = 0$ the optimal streamwise roll velocity necessarily decreases.

smaller threshold value, $\{I_u\} = 0.46\,\%$, for the SSST instability at $R_\delta^* = 1200$ is at least consistent with the experimental observations because in developing boundary layers the streamwise RGP occurs over the perturbation trajectory at Reynolds numbers smaller than $R_\delta^* = 1200$. Moreover, as shown above, initial conditions would typically play a central role in determining the transition scenario in experiments.

A feature of the development of the streamwise roll and streak structure at finite amplitude, seen in figure 20, is a pronounced asymmetry between the low- and high-speed streaks, in which the low-speed streak is notably enhanced. This enhancement, which is also seen in observations (Hernon, Walsh & McEligot 2007), helps to explain the prominence of low-speed streaks in the dynamics of transition. This asymmetry is also obtained when optimal streak perturbations are evolved nonlinearly (cf. Andersson *et al.* 2001) and is reflected in the structure of the exact nonlinear solutions found in plane shear flows (cf. Waleffe 1998). The fact that this asymmetry is obtained in the SSST framework establishes that inclusion of the full nonlinearity is not required for its explanation.
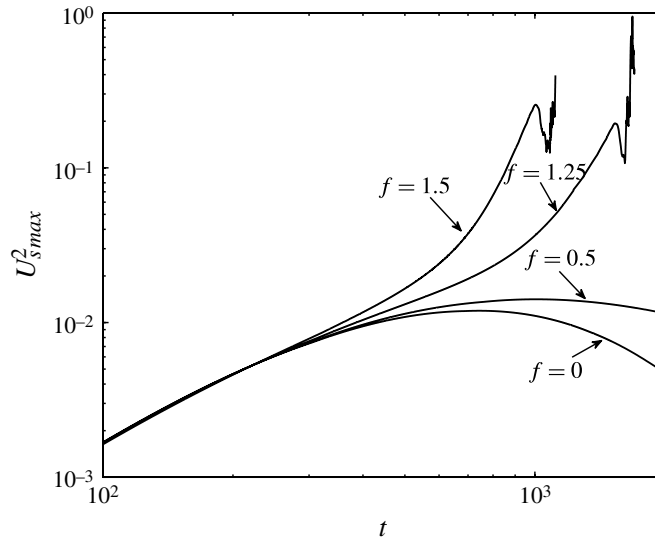
FIGURE 19. Development of the global energy optimal in Blasius flow at $R_{\delta*} = 1200$ in the presence of four levels of perturbation forcing amplitude. The global optimal perturbation at $m_{opt} = 0.51$ (cf. figure 17b,c) is excited at r.m.s. velocity 0.1 % of the free stream velocity, U_∞, in the presence of turbulence with $f = 0, 0.5, 1.25, 1.5$, all at perturbation streamwise wavenumber $k = 0.51$. Shown is the square of the maximum streak velocity. This Blasius flow is structurally stable at $m_{opt} = 0.51$ for $f < f_u \approx 0.8$ so that for $f = 0.5$ the streak initially grows but then decays, albeit with its rate of decay reduced by interaction with the turbulence. The profile is structurally unstable for $f > f_u$ and therefore for $f = 1.25$ and $f = 1.5$ the streak grows exponentially leading to transition to the time-dependent state. This figure demonstrates that the interaction between forced turbulence and an optimal initial condition in the Blasius flow converts the transiently growing initial condition into a SSST eigenmode and for $f > f_u$ into an unstable eigenmode which necessarily leads to transition.

Although the streaks reach large amplitude they produce modest change in the spanwise- and streamwise-averaged flow, $[U]$, prior to establishment of the time-dependent state, as shown in figure 21. Similar small variations in $\Delta U = U - [U]$ have been observed, prior to transition, in developing boundary layers subjected to FST (Westin *et al.* 1994; Matsubara & Alfredsson 2001), and in boundary layers with developing optimal streaks (Cossu & Brandt 2002).

The linear followed by nonlinear two-stage growth process leading to transition, in which the linear optimal provides the initial condition for the growth of the structural instability, serves to explain the observation that streamwise roll initial conditions, which decay in amplitude in the absence of FST, grow in the presence of FST (Alfredsson & Matsubara 1996; Bakchinov *et al.* 1997; Westin *et al.* 1998).

7. Transition to the time-dependent state in Couette flow

We saw that for an $f > f_c$ in Couette flow the spanwise uniform equilibrium becomes structurally unstable, giving rise to a growing streamwise roll and streak mode. This instability evolves into a finite-amplitude stable streamwise roll and streak equilibrium for $f_c < f < f_u$, but for $f > f_u$ fails to equilibrate, instead transitioning directly to a time-dependent state. Failure of continuation algorithms to find an equilibrium solution for $f > f_u$, and the absence of limit cycle behaviour, indicates that the transition to the time-dependent state for $f > f_u$ is through a saddle-node
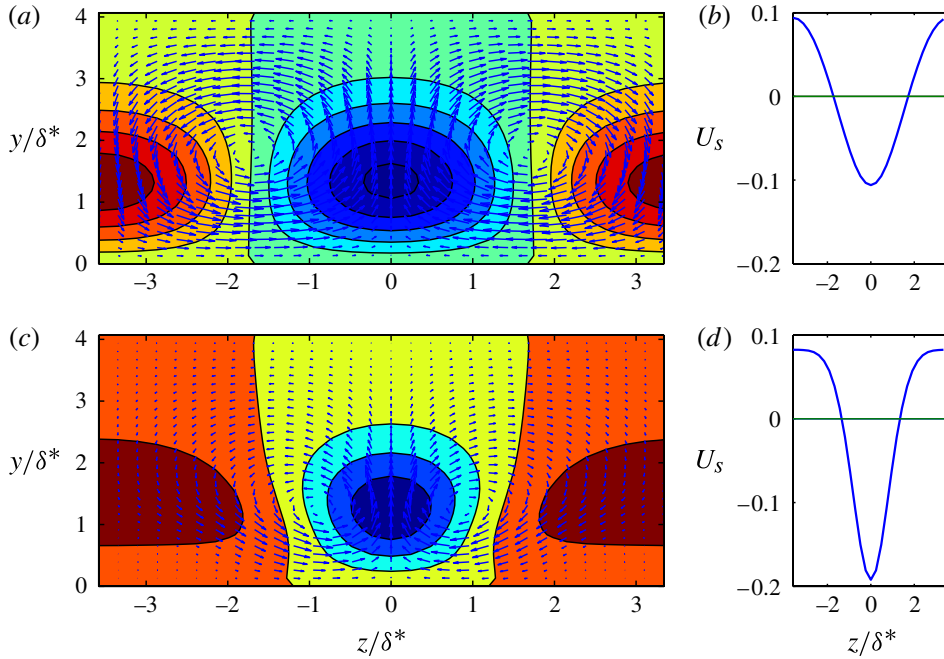
FIGURE 20. (Colour online) Development of the global optimal structure in Blasius flow at $R_{\delta*} = 1200$ in the absence of forced turbulence (a,b) and with forced turbulence (c,d). The global optimal perturbation at $m_{opt} = 0.51$ (cf. figure 17b,c) is excited at r.m.s. velocity 0.1 % of the free stream velocity, U_∞. (a) Snapshot at $t = 800$ of the streamwise-averaged streamwise flow, $U(y, z)$ (contours) and streamwise roll velocities, (V, W) (vectors) for $f = 0$ (cf. figure 19). Consistent with the lift-up mechanism, positive V is associated with a decrease in U. (b) The corresponding streak velocity, $U_s = U - [U]$, at the level of its maximum $y/\delta^* = 1.31$. (c) The corresponding snapshot at $t = 800$ for $f = 1.25$ and $k = 0.51$. (d) The corresponding streak velocity at the level of its maximum, $y/\delta^* = 1.18$. The velocities are normalized by U_∞ and other parameters are as in figure 19. The nonlinearity retained in SSST dynamics predicts the marked enhancement of the low-speed streak at this time prior to transition.

bifurcation. Saddle-node bifurcations have also been associated with exact coherent structures (i.e. Nagata 1990, 1997; Waleffe 1998, 2001, 2003; Halcrow *et al.* 2009) and low-order models (i.e. Waleffe 1997).

The streamwise roll and streak equilibria for $f_c < f < f_u$ are hydrodynamically stable even when highly inflected. As f approaches f_u the perturbation field is increasingly dominated by the sinuous mode. For $f > f_u$, as shown in figure 22 for evolution of the streamwise roll and streak with $f = 8.2$, the flow transitions to a time-dependent state, coincident with the streak becoming hydrodynamically unstable. This scenario of transition is consistent with the streak breakdown mechanism (Reddy *et al.* 1998).

Streamwise roll and streak structures during the transition to, and establishment of, the time-dependent state are shown in figure 23. The streamwise flow, with streak spacing $z^+ \approx 50$, transitions to a time-dependent state, with streak spacing $z^+ \approx 100$, which is characterized by streak collapse occurring at irregular intervals (panel for $t = 600$). This time-dependent state is similar to the self-sustaining state seen in minimal channel turbulence simulations (Jiménez & Moin 1991; Hamilton *et al.* 1995), and the streak-spacing of $z^+ \approx 100$ also agrees with observations (Smith & Metzler 1983; Komminaho *et al.* 1996).
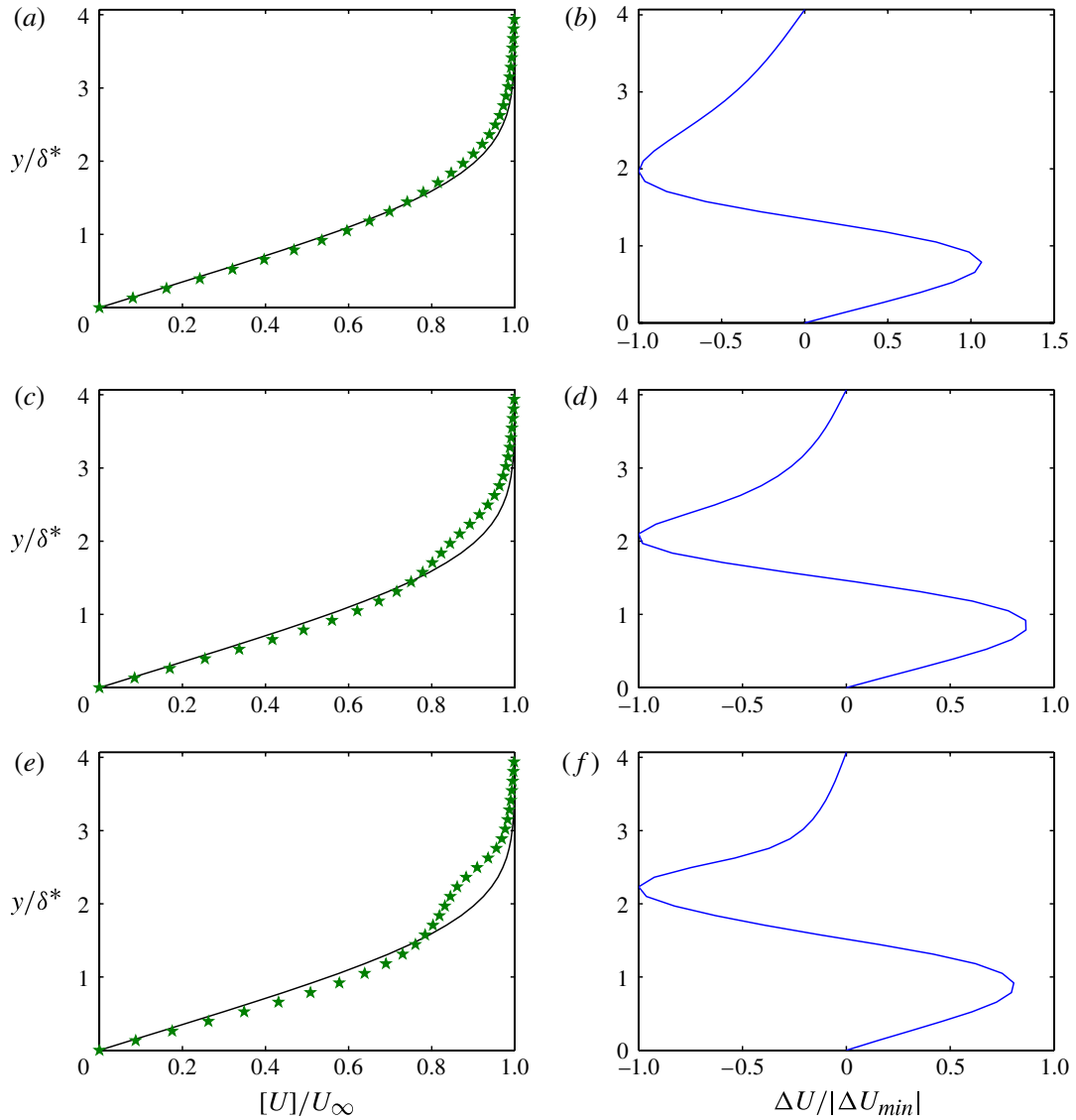
FIGURE 21. (Colour online) Streamwise velocity defect resulting from the development of the global energy optimal in Blasius flow at $R_{\delta*} = 1200$. The global optimal perturbation at $m_{opt} = 0.51$ (cf. Figure 17b,c) is excited at r.m.s. velocity 0.1 % of the free stream velocity, U_∞. The turbulence is forced at $k = 0.51$ with $f = 1.25$. (a,c,e) Spanwise-averaged streamwise velocity for the optimal streamwise roll and streak evolution shown in figure 19 (stars). For comparison, the associated Blasius boundary layer flow profile is also shown (solid). (b,d,f) Difference between the spanwise-averaged streamwise velocity and the Blasius profile. This defect is normalized by the magnitude of its minimum value. This figure shows that development of the optimal streamwise roll and streak in SSST, prior to transition, induces small changes in the boundary layer profile that are consistent with observations (cf. Westin *et al.* (1994), their figure 7): (a) $t = 1300$; (b) $|\Delta U_{min}| = 0.025$; (c) $t = 1500$; (d) $|\Delta U_{min}| = 0.057$; (e) $t = 1560$; (f) $|\Delta U_{min}| = 0.083$.

This time-dependent state is self-sustaining in the sense that it persists if the forcing is removed, by setting $f = 0$.
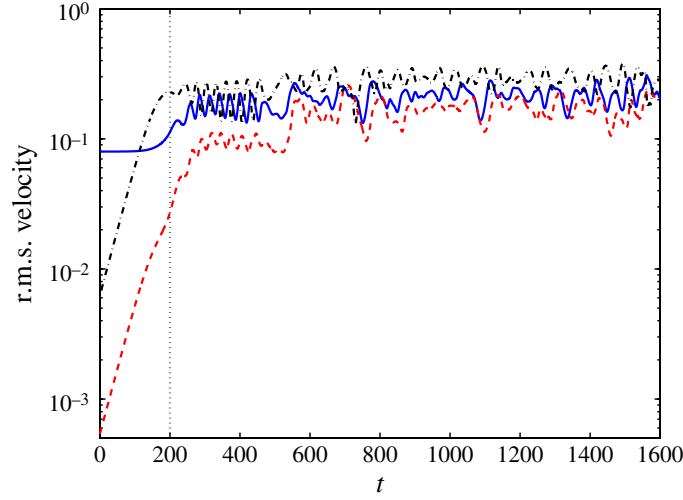
FIGURE 22. (Colour online) Structural instability induced transition to the time-dependent state starting from Couette flow. Shown are r.m.s. perturbation velocity (solid), r.m.s. roll velocity (dashed) and r.m.s. streak velocity (dash-dot). The dotted line at $t = 200$ marks the time when the instantaneous streamwise-averaged flow first becomes hydrodynamically unstable. The perturbation forcing amplitude is $f = 8.2$ and other parameters are as in figure 3.

8. The minimal self-sustaining turbulence dynamics obtained from SSST

An important property of the self-sustaining state, with $f = 0$, in SSST is that the covariance, $\boldsymbol{C}_k$, collapses to rank one. Collapse to rank one of $\boldsymbol{C}_k$ results from the fact that the Lyapunov equation:

$$\frac{\mathrm{d}\boldsymbol{C}_k}{\mathrm{d}t} = \boldsymbol{A}_k(\boldsymbol{U})\boldsymbol{C}_k + \boldsymbol{C}_k\boldsymbol{A}_k^\dagger(\boldsymbol{U}) \tag{8.1}$$

in the absence of stochastic forcing and with given $\boldsymbol{U}(t)$, admits as a solution the rank-one covariance, $\boldsymbol{C}_k = \hat{\boldsymbol{\phi}}_k\hat{\boldsymbol{\phi}}_k^\dagger$, in which $\hat{\boldsymbol{\phi}}_k$ evolves according to

$$\frac{\mathrm{d}\hat{\boldsymbol{\phi}}_k}{\mathrm{d}t} = \boldsymbol{A}_k(\boldsymbol{U})\hat{\boldsymbol{\phi}}_k. \tag{8.2}$$

In (8.2) all initial states, $\hat{\boldsymbol{\phi}}_k$, evolve asymptotically to the first Lyapunov vector and this happens for every k. It follows that all full-rank covariances will asymptotically approach rank one. Consequently, the SSST dynamics with $f = 0$ reduce to the nonlinear interaction between the first Lyapunov vector for each k and the streamwise-averaged flow, governed by

$$\frac{\mathrm{d}\hat{\boldsymbol{\phi}}_k}{\mathrm{d}t} = \boldsymbol{A}_k(\boldsymbol{U})\hat{\boldsymbol{\phi}}_k, \tag{8.3a}$$

$$\boldsymbol{C}_k = \hat{\boldsymbol{\phi}}_k\hat{\boldsymbol{\phi}}_k^\dagger, \tag{8.3b}$$

$$\frac{\mathrm{d}\boldsymbol{\Gamma}}{\mathrm{d}t} = \boldsymbol{G}(\boldsymbol{\Gamma}) + \sum_k \mathrm{Re}(\boldsymbol{L}_{RS}\boldsymbol{C}_k), \tag{8.3c}$$
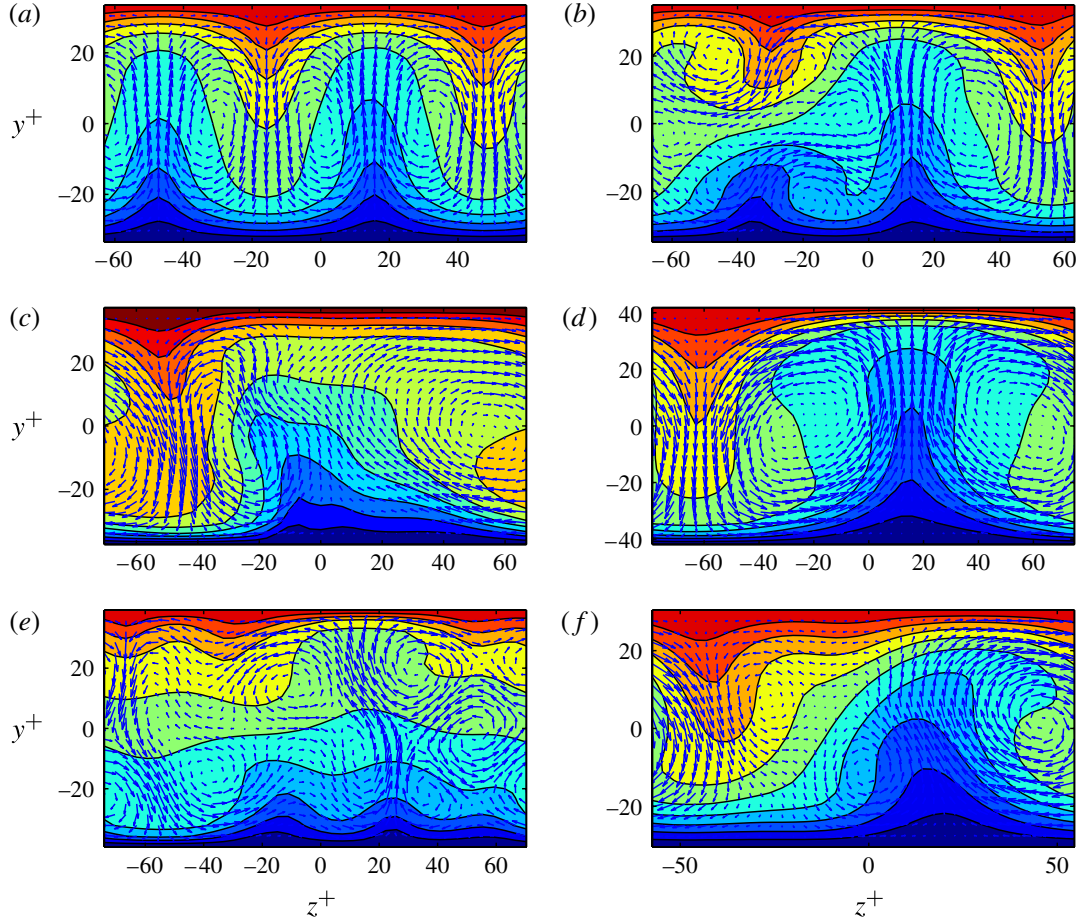
where the operators in (8.3) are as in (3.21).

FIGURE 23. (Colour online) Streamwise roll and streak structure during the transition to, and establishment of, the time-dependent state shown in figure 22. Snapshots are shown of the streamwise-averaged streamwise flow (contours), and vectors of the streamwise-averaged cross-stream/spanwise flow. Consistent with the lift-up mechanism, positive V is associated with a decrease in U. At $t = 200$, the streamwise flow has just become perturbation unstable. Channel distances are measured in wall units, revealing the time-dependent state to be characterized by streaks with mean spacing of about $z^+ = 100$. The streak episodically collapses (cf. the figure for $t = 600$), and reforms. The contour interval is 0.2: (a) $t = 200$; (b) $t = 300$; (c) $t = 400$; (d) $t = 500$; (e) $t = 600$; (f) $t = 860$.

We wish to show using SSST that the self-sustaining state naturally produces a minimal representation of turbulence in wall-bounded shear flow in the sense that the dynamics is limited to the interaction of the streamwise-averaged flow with a small number of streamwise harmonic perturbations. In the self-sustaining state, with $f = 0$, we have shown that for each k in (8.3a) an initially full-rank covariance, $\boldsymbol{C}_k$, collapses under SSST dynamics to the rank-one covariance $\boldsymbol{C}_k = \hat{\boldsymbol{\phi}}_k \hat{\boldsymbol{\phi}}_k^\dagger$, with $\hat{\boldsymbol{\phi}}_k$ the Lyapunov vector associated with its first Lyapunov exponent, $\lambda_k = \lim_{t \to \infty} (1/t) \ln |\hat{\boldsymbol{\phi}}_k(t)|$. Moreover, if the largest λ_k is attained at a single streamwise k, the perturbation energy will become progressively concentrated in this single wavenumber associated with the largest λ_k, which is necessarily $\lambda_k = 0$, consistent with a bounded solution trajectory.
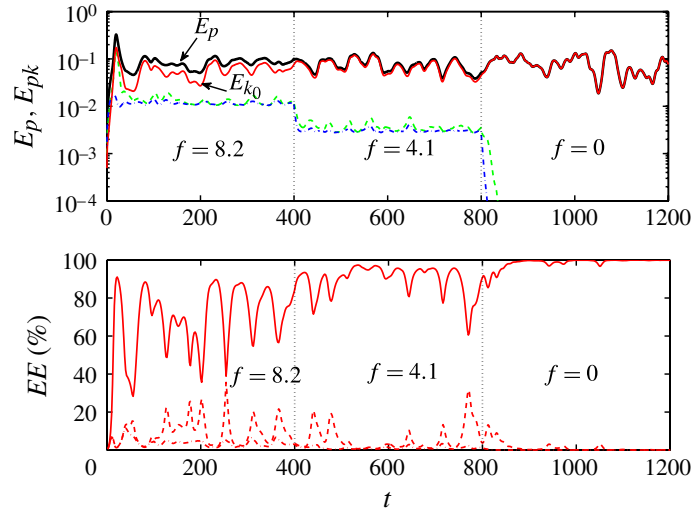
FIGURE 24. (Colour online) Perturbation complexity decrease associated with establishment of the minimal self-sustaining state as $f \to 0$. The time-dependent state is initialized with perturbation forcing amplitude $f = 8.2$ and zero covariance. Subsequently, f is decreased to $f = 4.1$ at $t = 400$ and to $f = 0$ at $t = 800$, after which time the state is unforced and self-sustaining. (*a*) Fraction of the total perturbation energy (top solid) accounted for by streamwise wavenumbers k_0 (solid), $2k_0$ (dashed), and $3k_0$ (dash-dot), with $k_0 = 1.143$. For $t > 800$ in this log plot, suppression of the subdominant perturbations at streamwise wavenumbers $2k_0$ and $3k_0$ is indicated by their exponential decay at the rate of their negative Lyapunov exponents, while the dominant k_0 component necessarily has the zero Lyapunov exponent of the state trajectory. This plot reveals complete dominance of the k_0 perturbation in the self-sustaining state subsequent to $t = 800$. (*b*) Fraction of perturbation energy in each of the first three empirical eigenfunctions associated with the dominant streamwise wavenumber, $k_0 = 1.143$ (first *EE*: solid; second *EE*: dashed; third *EE*: dash-dot). Simultaneous with the concentration of perturbation structure in the single streamwise wavenumber, k_0, is the collapse of the covariance to rank one at this wavenumber. The collapse of the state to rank one is complete for $f = 0$, but even for $f = 8.2$, which parameterizes strong perturbation/perturbation nonlinearity, the tendency for reduction of the perturbation state to a single structure remains robust. Here $R = 400$, and other parameters are as in figure 3. This figure reveals that this self-sustaining state is intrinsically associated with a minimal representation of turbulence.

Transition to this minimal dynamics is demonstrated by considering the SSST system (3.21) for Couette channel flow at $R = 400$ with equal forcing at the three perturbation wavenumbers: $[k/2, k, 2k]$ with $k = 1.143$ and with perturbation forcing amplitude, $f_k = 8.2$ for each wavenumber. Spanwise symmetry of the Couette flow is broken with a small initial streak perturbation. The result of such an experiment is shown in figure 24. The system rapidly transitions to a time-dependent state with perturbation energy distributed among all structures. However, when the perturbation forcing amplitude, f_k, is reduced to zero, at $t = 800$, so that the system becomes fully self-sustaining, the perturbation energy becomes concentrated in the single streamwise wavenumber $k = 1.143$, as shown in figure 24 (top and middle panels). Moreover, this collapse of perturbation energy to $k = 1.143$, is accompanied by the collapse of the associated covariance, $\mathbf{C}_k$, to rank one, as shown in figure 24 (bottom panel). This collapse is consistent with the emergence of the dominant Lyapunov vector associated with (8.3*a*), as discussed above.
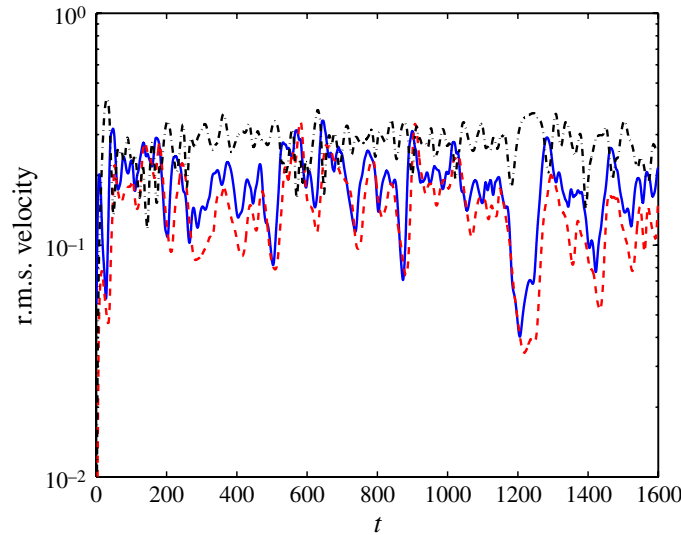
FIGURE 25. (Colour online) Initial condition induced transition to the self-sustaining state starting from Couette flow. Shown are r.m.s. perturbation velocity (solid), r.m.s. streamwise roll velocity (dashed) and r.m.s. streak velocity (dash-dot). This figure demonstrates that transition to the self-sustaining state can be induced by an initial condition in the absence of externally forced turbulence. This self-sustaining state is maintained by the nonlinear interaction between the streamwise-averaged flow and a single streamwise harmonic perturbation. The initial condition is a $t = 10$ energy growth optimum at $k = 1.143$ excited with r.m.s. velocity 6.8 % of U_0. The perturbation forcing amplitude is $f = 0$ and other parameters are as in figure 3.

This perturbation covariance rank collapse at k_0 demonstrates how this self-sustaining turbulent state dynamics naturally reduces to a single time-dependent perturbation structure interacting with the mean flow, providing a minimal representation of shear flow turbulence. It also suggests a mechanism by which a dominant coherent structure arises in turbulence and identifies this structure with the first Lyapunov vector of (8.3a), together with the associated streamwise-averaged flow. While nonlinear interaction among perturbations opposes this rank collapse in the full equations, this mechanism of rank collapse remains robust and helps explain the tendency for a small number of coherent structures to dominate the variance in wall-bounded shear flow turbulence, as has often been remarked (Berkooz, Holmes & Lumley 1993).

We now demonstrate the establishment and maintenance of a self-sustaining state by perturbing the Couette flow at $R = 400$ with the $t = 10$ energy growth optimal perturbation at $k = 1.143$. This optimal, when introduced at r.m.s. amplitude 6.8 % of U_0, results in rapid transition to a self-sustaining state, as shown in figure 25. This self-sustaining state, the structure of which is shown in figure 26, is essentially similar to the time-dependent state obtained with stochastic forcing included, shown in figure 23.

This minimal turbulence dynamics accurately approximates many aspects of Couette flow turbulence. In figure 27 we plot the projection of the turbulent state on the plane of the non-dimensional energy input rate,

$$I \equiv \frac{1}{R} \frac{1}{2L_y} \left([U(1)] \left. \frac{d[U]}{dy} \right|_{y=1} - [U(-1)] \left. \frac{d[U]}{dy} \right|_{y=-1} \right), \tag{8.4}$$
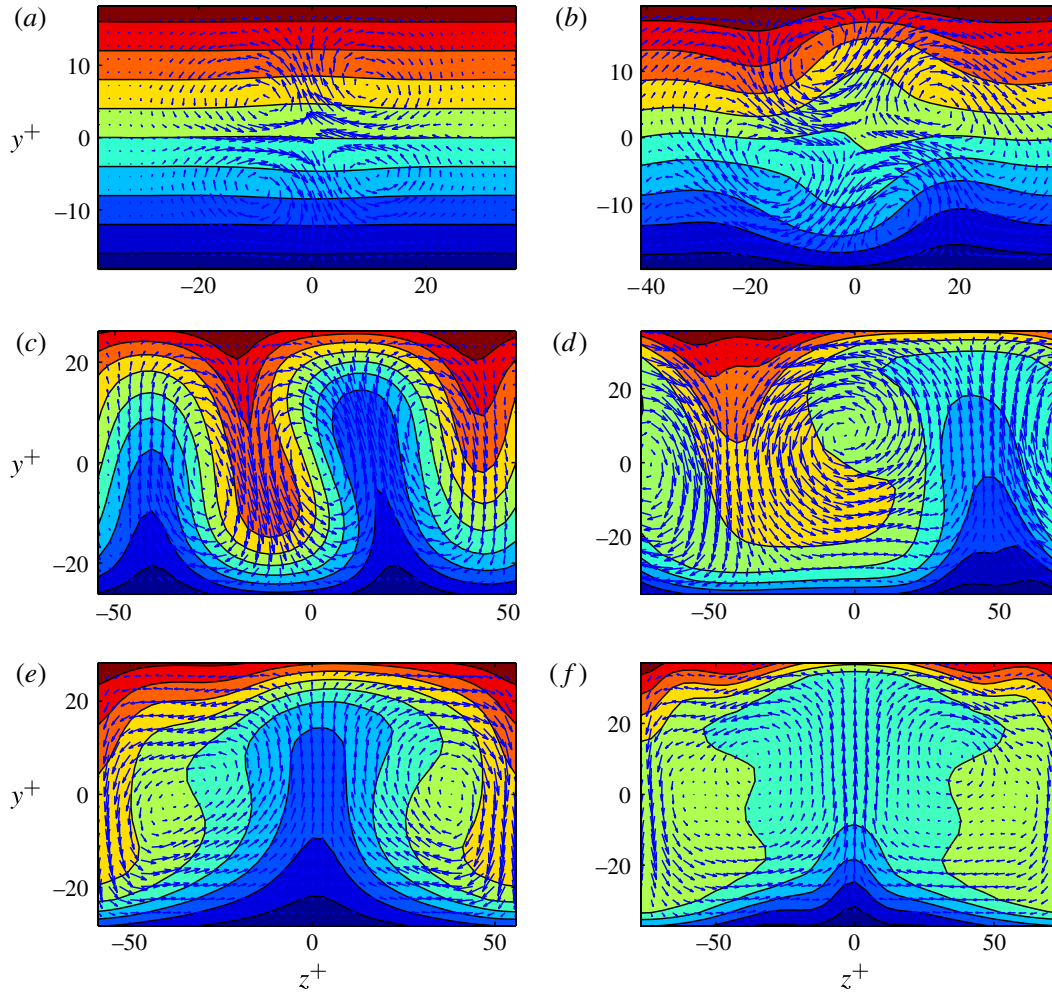
FIGURE 26. (Colour online) Streamwise roll and streak structure during the transition to, and establishment of, the time-dependent state shown in figure 25. Snapshots are shown of the streamwise-averaged streamwise flow (contours), and vectors of the streamwise-averaged cross-stream/spanwise flow. Consistent with the lift-up mechanism, positive V is associated with a decrease in U. Channel distances are measured in wall units, revealing the time-dependent state to be characterized by streaks with mean spacing of about $z^+ = 100$. At $t = 30$, the streamwise-averaged flow has just become hydrodynamically unstable. The streak episodically collapses (cf. the figure for $t = 1280$), and reforms. The contour interval is 0.2: (*a*) $t = 2$; (*b*) $t = 10$; (*c*) $t = 30$; (*d*) $t = 200$; (*e*) $t = 1250$; (*f*) $t = 1280$.

and the non-dimensional energy dissipation rate, D, given by (4.5). This trajectory is consistent with the I/D trajectory obtained in simulations of Couette flow turbulence (Kawahara & Kida 2001; Gibson, Halcrow & Cvitanović 2008). Further, the mean streamwise flow maintained by this minimal self-sustaining state at $f = 0$, as well as by the SSST state at $f = 8.2$, which are shown in figure 28, are close to that obtained in simulations (Kawahara & Kida 2001). The corresponding cross-stream distributions of the mean r.m.s. perturbation velocities for this minimal self-sustaining state, shown in figure 29, are also similar to these distributions simulated under turbulent conditions (Kawahara & Kida 2001). These comparisons verify that fundamental features of turbulence are captured by this minimal self-sustaining state.
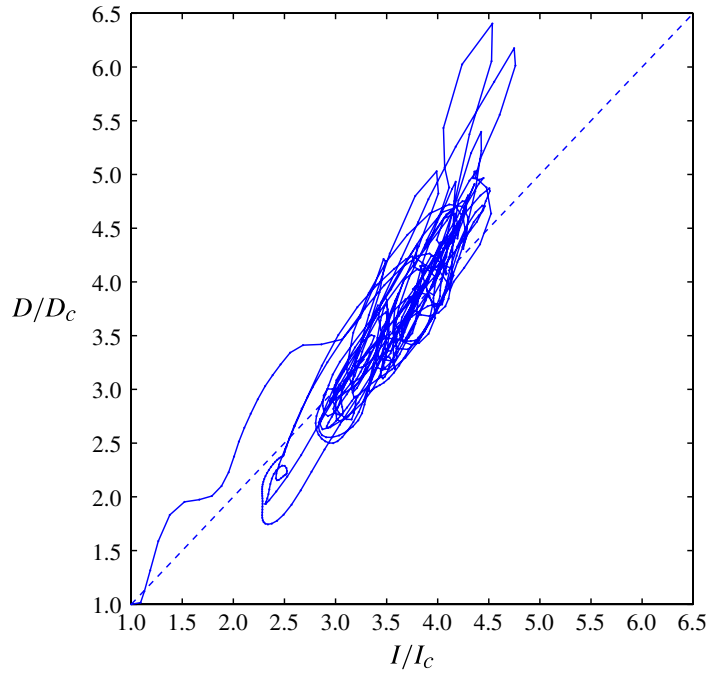
FIGURE 27. (Colour online) Trajectory of the self-sustaining state shown in figure 25 on the plane of the energy input rate, I, and the energy dissipation rate, D. The trajectory begins at Couette flow (lower left point in trajectory) and settles into a transient chaotic trajectory with values of I and D typical of turbulence. Both I and D have been normalized by the value for laminar Couette flow. This figure demonstrates that the self-sustaining state I/D plane trajectory is consistent with simulations of Couette flow turbulence.

9. The parametric mechanism maintaining the self-sustaining state

We wish to gain a clearer understanding of the physical mechanism supporting the self-sustaining state. The robust tendency for streaks to organize the perturbation field producing Reynolds stresses supporting the streak, via the lift-up mechanism, was illustrated in connection with the streak perturbations shown in figure 3. This tendency also produces the SSST streamwise RGP illustrated in figure 1. Although the streak is strongly fluctuating in the self-sustaining state, this tendency of the streak to organize oblique supporting perturbations is retained as illustrated in figure 30. The time derivative of the domain average square streamwise vorticity, $\mathrm{d}/\mathrm{d}t(\int \mathrm{d}y\,\mathrm{d}z\Omega_x^2/(2L_yL_z))$ with $\Omega_x = W_y - V_z$, provides a measure of the streamwise roll forcing. A times series of this diagnostic is also shown in figure 30. It is remarkable that the perturbations, in this highly time-dependent state, produce streamwise vorticity forcing maintaining the streamwise roll not only on average but at nearly every instance of time.

This robust tendency for perturbation Reynolds stresses to maintain the streak through the lift-up mechanism explains the maintenance of the streamwise roll and streak structure by the perturbations. However, maintenance of the perturbations in the self-sustaining state remains to be explained. It is tempting to appeal to hydrodynamic instability of the time-dependent streak to explain the maintenance of the perturbations (Hamilton *et al.* 1995; Waleffe 1997). Indeed, eigenanalysis of the instantaneous streamwise-averaged flow reveals that instability would occur, assuming the flow time-dependence could be ignored, as can be seen from the maximum mode growth rates shown in figure 31. However, this instability is only notional as its growth rate time
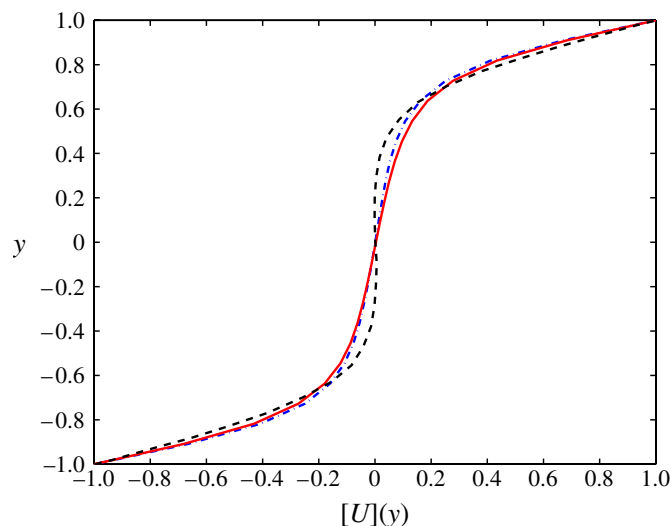
FIGURE 28. (Colour online) Spanwise- and time-averaged streamwise flow, $[U](y)$, for the self-sustaining state shown in figure 25 (solid), and for the time-dependent state with perturbation forcing amplitude $f = 8.2$, shown in figure 22 (dash-dot). For comparison, the spanwise- and time-averaged streamwise flow from the simulation of Kawahara & Kida (2001) at the same Reynolds number is shown (dashed). This figure demonstrates that both the self-sustaining state and the time-dependent state with forced turbulence produce a streamwise-averaged flow profile consistent with simulations of Couette flow turbulence.
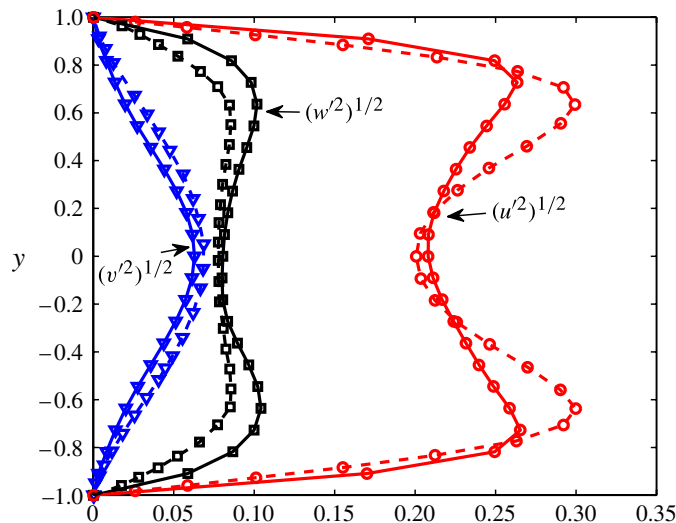

FIGURE 29. (Colour online) Cross-stream distribution of spanwise- and time-averaged perturbation statistics for the self-sustaining state in figure 25. Shown are spanwise- and time-averaged r.m.s.: streamwise velocity $\sqrt{\langle u^2 \rangle}$ (solid circles), cross-stream velocity $\sqrt{\langle v^2 \rangle}$ (solid triangles) and spanwise velocity $\sqrt{\langle w^2 \rangle}$ (solid squares). For comparison, the time and spanwise mean flows from the simulation of Kawahara & Kida (2001) at the same Reynolds number are also shown (dashed). Velocities are normalized by the maximum Couette flow velocity. This figure demonstrates that the self-sustaining state produces turbulent velocity statistics consistent with simulations of Couette flow turbulence.
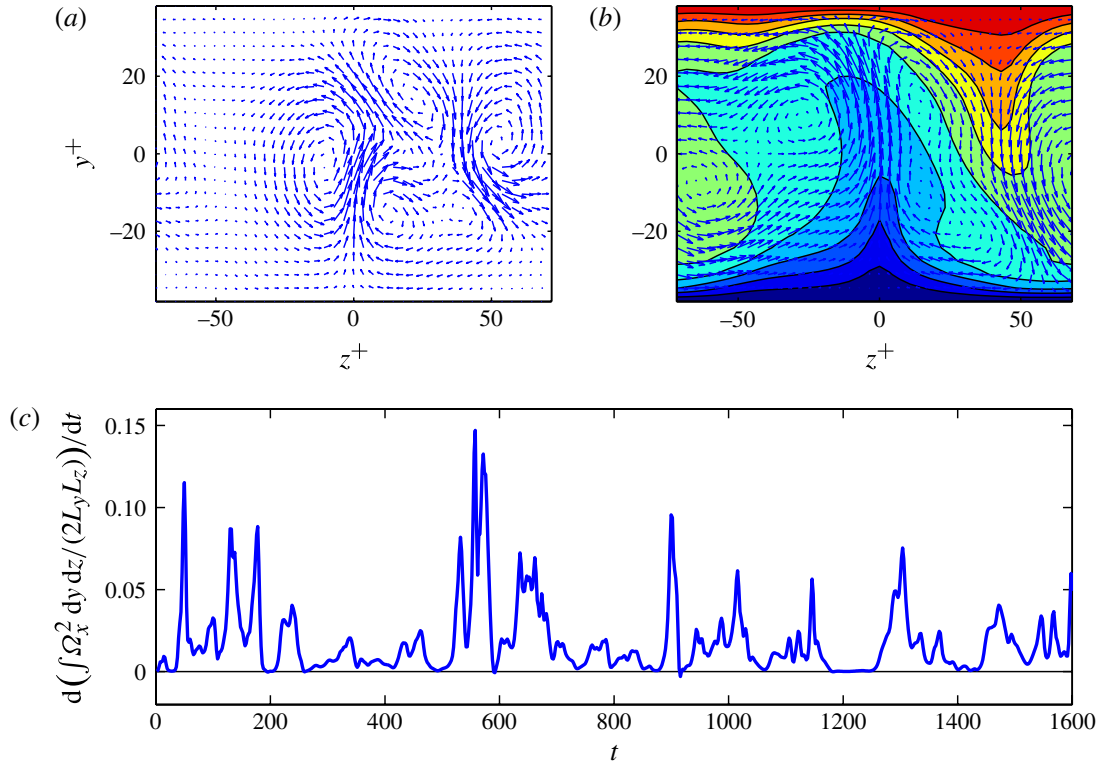
FIGURE 30. (Colour online) Streamwise roll forcing by perturbation Reynolds stresses in the self-sustaining state shown in figure 25. (*a*) Vectors of instantaneous cross-stream/spanwise velocity acceleration, $(\dot{V}, \dot{W})$, at time $t = 980$. (*b*) Streamwise roll and streak structure at the same time. (*c*) Time series of streamwise roll forcing as indicated by the rate of change of the average square streamwise vorticity. It is remarkable that the perturbations, in this highly time-dependent state, produce streamwise roll forcing, not only on average, but also at nearly every instance of time.

scale, $\tau = 1/\sigma_r \approx 25$, is the same as the growth rate correlation time, $\tau = 25$ (cf. figure 31). Moreover, perturbation growth rate is weakly associated with unstable mode growth rate, as can be seen from comparison of their respective time series, or from a scatter plot of these growth rates, both shown in figure 31.

Therefore, it appears that the perturbations are not sustained by modal instability. In order to test this, an integration of a turbulent state at $R = 800$ was performed with the instantaneous flow enforced to be stable by setting all eigenvalues, $(\sigma_r + i\sigma_i)$, with $\sigma_r > 0$ to $(-0.001 + i\sigma_i)$ at each time step. Despite suppression of all instability, the time-dependent state continues to be self-sustaining. Persistence of the self-sustaining state is verified by time series obtained after this intervention, shown in figure 32. In fact, it can be seen from figure 32 that the streak is stronger in the stabilized self-sustaining state than it is in the non-stabilized state, which is consistent with reduced energy extraction from the streak when instability is suppressed.

This experiment shows that, in the self-sustaining state, perturbation energy is maintained by a growth mechanism that is unrelated to modal instability (cf. Schoppa & Hussain 2002). We wish to gain an understanding of this mechanism. Despite the lack of modal instability, perturbations are still able to extract energy through non-normal interaction with the mean state, but in a stable, time-independent flow
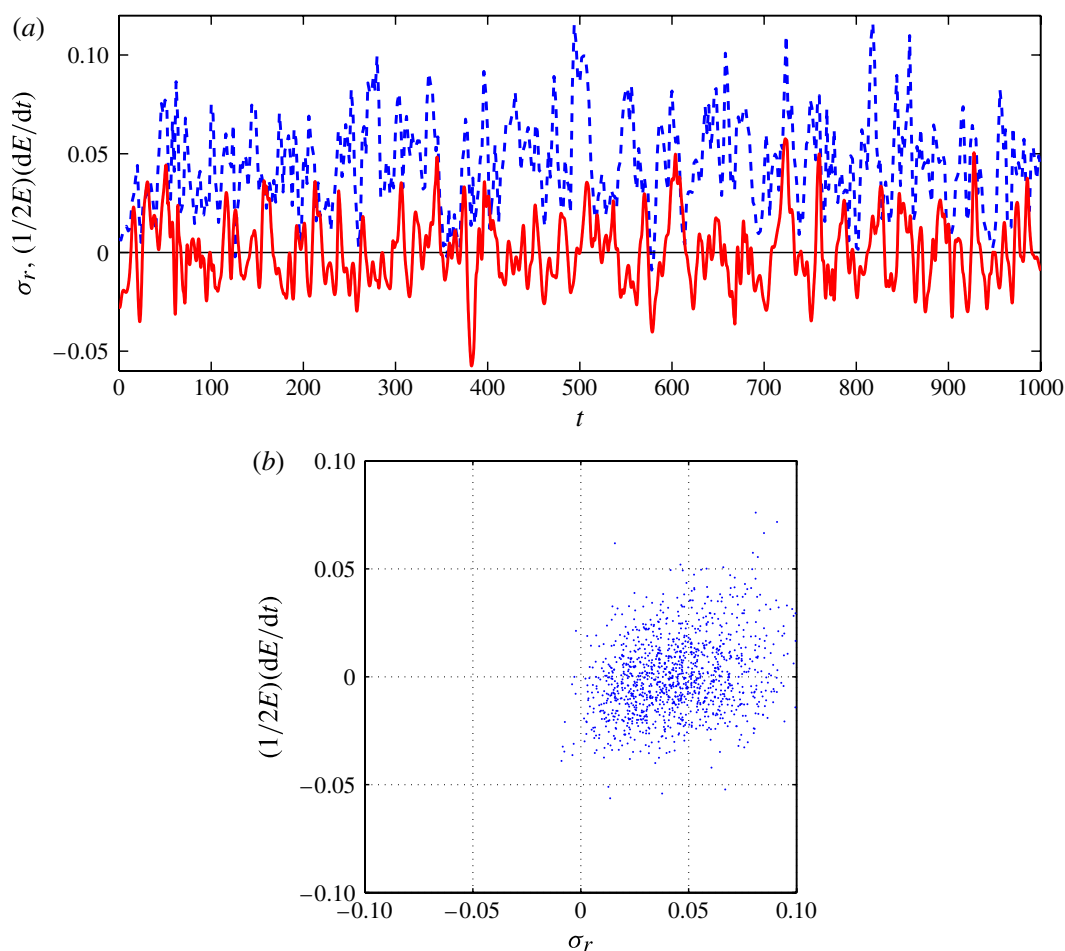
FIGURE 31. (Colour online) Comparison between perturbation growth rate and modal growth rate for the self-sustaining state in figure 25. (*a*) Maximum mode growth rate (dashed), σ_r, and perturbation growth rate (solid), $(1/2E)\,\mathrm{d}E/\mathrm{d}t$. (*b*) Scatter plot of these growth rates. The temporal correlation time of σ_r is $\tau_c = 25$, and the mean of σ_r is 0.04. The correlation coefficient between these growth rates over the whole simulation is 0.2. This figure indicates that maintenance of the perturbation energy in the self-sustaining state is not significantly related to streak instability.

the resulting perturbation growth, however large, is ultimately transient and could not maintain the perturbation field. In the example of figure 32, the system is stable and, if it were not time dependent, the perturbations would ultimately decay and the flow would laminarize to the Couette flow. It is a remarkable fact that, in time-dependent dynamical systems, the non-normal growth, which would be transient in a time-independent system, can be sustained to produce exponential growth through an essentially non-normal parametric mechanism (Farrell & Ioannou 1996*b*, 1999; Pedlosky & Thomson 2003; Poulin *et al.* 2003; Farrell & Ioannou 2008*b*; Poulin *et al.* 2010). This non-normal parametric growth process underlies the instability of a damped harmonic oscillator with periodically varying restoring force, a system which, like the stabilized system example described above, is non-normal, time-dependent and modally stable at every instance of time.
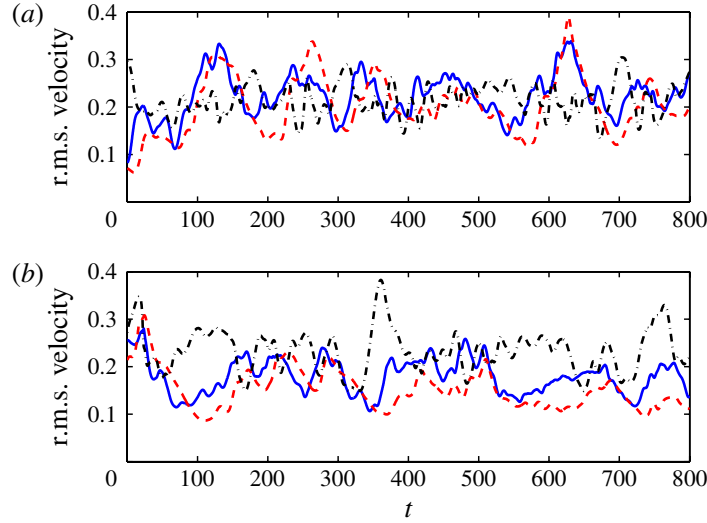
FIGURE 32. (Colour online) Self-sustaining state at $R = 800$ with and without modal instability. (*a*) The self-sustaining state time evolution in the variables r.m.s. perturbation velocity (solid), r.m.s. roll velocity (dashed) and r.m.s. streak velocity (dash-dot). (*b*) The same variables for the stabilized self-sustaining state. This state was made stable at every instance of time in the following manner: all unstable eigenfunctions were ascribed growth rate -0.001 while their phase speed and structure were left unchanged. The turbulence is unforced, $f = 0$, and other parameters are as in figure 3. Suppression of modal instability results in a self-sustaining state with stronger rather than weaker streaks. This figure demonstrates that modal instability does not maintain perturbation variance in the self-sustaining state.

This non-normal parametric growth mechanism can be illustrated by projecting the perturbation states, $\hat{\boldsymbol{\phi}}_k$, associated with the self-sustaining states shown in figures 25 and 26, on the instantaneous directions of energy growth. To facilitate calculating this diagnostic, transform the perturbation state to $\boldsymbol{\psi}_k \equiv \boldsymbol{M}_k^{1/2} \hat{\boldsymbol{\phi}}_k$ and the perturbation dynamics to

$$\frac{\mathrm{d}\boldsymbol{\psi}_k}{\mathrm{d}t} = \tilde{\boldsymbol{A}}_k \boldsymbol{\psi}_k, \tag{9.1}$$

with $\tilde{\boldsymbol{A}}_k \equiv \boldsymbol{M}_k^{1/2} \boldsymbol{A}_k(\boldsymbol{U}(t)) \boldsymbol{M}_k^{-1/2}$ (cf. Appendix). Perturbation energy growth directions are those associated with positive eigenvalues of the Hermitian matrix, $\boldsymbol{D} = \tilde{\boldsymbol{A}}_k + \tilde{\boldsymbol{A}}_k^{\dagger}$, while decay directions are associated with negative eigenvalues (Farrell & Ioannou 1996*a*,*b*). Therefore, the instantaneous growth rate can be partitioned into contributions from orthogonal growing and decaying subspaces, spanned by the eigenvectors of $\boldsymbol{D}_g$ and $\boldsymbol{D}_d$, respectively:

$$\frac{1}{E_k} \frac{\mathrm{d}E_k}{\mathrm{d}t} = \frac{\boldsymbol{\psi}_k^{\dagger} \boldsymbol{D} \boldsymbol{\psi}_k}{\boldsymbol{\psi}_k^{\dagger} \boldsymbol{\psi}_k} = \frac{\boldsymbol{\psi}_k^{\dagger} (\boldsymbol{D}_g + \boldsymbol{D}_d) \boldsymbol{\psi}_k}{\boldsymbol{\psi}_k^{\dagger} \boldsymbol{\psi}_k}. \tag{9.2}$$

A plot with axes consisting of the sum of the projections of the perturbation state on the growing and on the decaying subspaces provides a two-dimensional trajectory of the system in the coordinates of growth rate and decay rate. Assuming the solutions of (8.3) are statistically steady, the time average perturbation growth rate is zero implying that the time average of the projections on the growing and decaying directions are

equal. This implies that the projection of the state lies, on average, along the diagonal in these coordinates, while a perturbation state maintained by a neutral mode would lie at a point on the diagonal. Time series representing the self-sustaining state trajectories with and without stabilization of modal instability of the instantaneous flow are shown in figures 32 and 33. These trajectories are essentially similar and because one of these systems is constrained to be always stable, we conclude that the perturbations in both of these systems are sustained by the time-dependent, non-normal, parametric growth process.

This SSP is illustrated in figure 2; the streak grows by organizing the perturbation Reynolds stresses to drive its associated streamwise roll while the perturbations are sustained by the parametric growth mechanism associated with the time dependence of the streak.

10. Summary and conclusion

Two fundamental problems in wall-bounded shear flow turbulence research are understanding the mechanism of transition from the laminar to the turbulent state in perturbation stable flows and understanding the mechanism maintaining the turbulent state, once it is established. In this work, we have used SSST, which provides a deterministic, autonomous, nonlinear dynamical system for evolving a second-order approximation to the statistical mean turbulent state, to study the dynamics of streamwise roll and streak interaction with turbulence in both transition to and maintenance of turbulence. Underlying the SSST dynamics are the assumptions that the perturbation–perturbation interactions and the external sources of turbulence in the perturbation equations can be parameterized as an additive stochastic forcing delta correlated in time and that the streamwise average of the perturbation covariance can be obtained from the ensemble average over realizations of the forcing.

Applied to the transition problem, SSST reveals a new instability arising from interaction between the streamwise rolls and streaks and forced turbulence. Prior to transition to freely maintained turbulence, forced turbulence is always present in naturally occurring wall-bounded shear flows, so that this interaction instability of the streamwise roll and streak is likely to influence transition in such natural settings. We showed that the SSST instability exploits the optimality of the lift-up mechanism by organizing perturbation Reynolds stresses to coherently force the streamwise roll. This robust process of Reynolds stress organization by the streak, resulting in forcing of the associated streamwise roll, provides the coupling between the streak and the streamwise roll required to produce modal instability from the powerful non-normal transient growth provided by the lift-up mechanism. This instability effectively transforms the otherwise transient growth of optimal or near-optimal perturbations arising in the forced turbulence into persistently growing modal streamwise roll and streak structures.

Linear optimal excitation theory accurately predicts the streamwise roll and streak structure seen in transitional boundary layers (Luchini 2000; Andersson *et al.* 2001). However, there may be insufficient forcing of the initial condition to produce transition before the eventual decay of the transiently growing streamwise roll and streak (Brandt *et al.* 2002). Indeed, localized streamwise roll and streak initial conditions are observed to decay in the presence of very low FST (Alfredsson & Matsubara 1996; Bakchinov *et al.* 1997; Westin *et al.* 1998). An alternative, and potentially complementary, mechanism is the formation of streamwise rolls and streaks from the nonlinear interaction of oblique waves (Benney 1960, 1984; Jang *et al.* 1986;
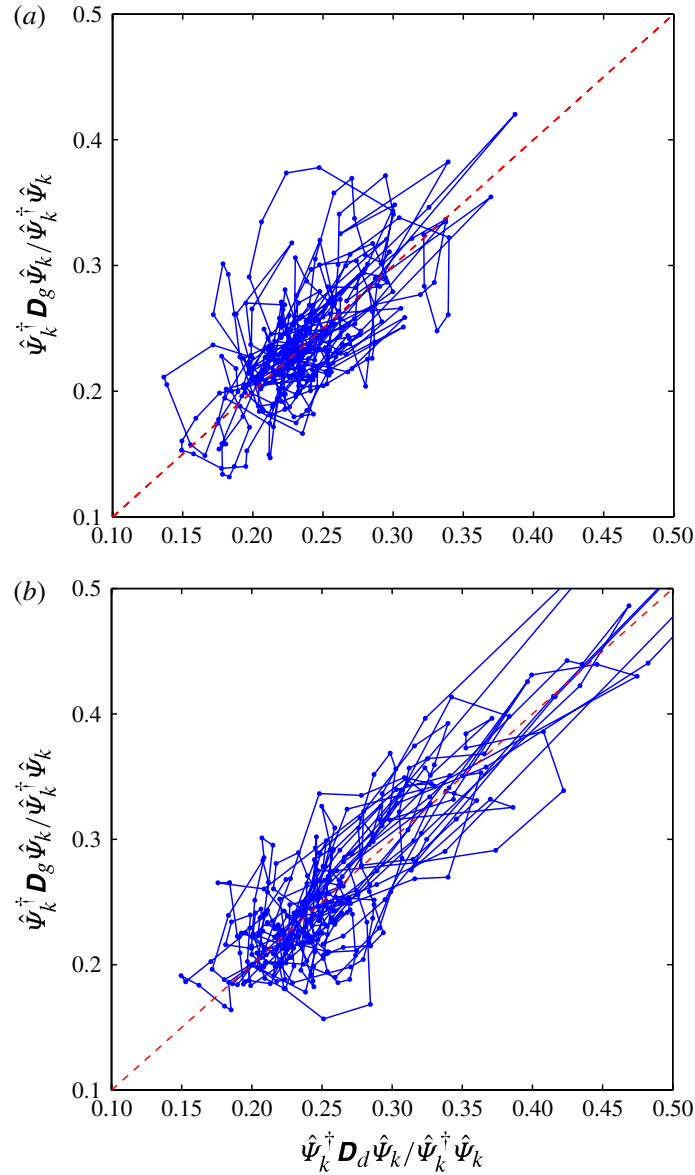
FIGURE 33. (Colour online) Trajectory of the self-sustaining state both with and without modal instability suppression. The coordinates are the projections of the state on the growing and on the decaying subspaces of the dynamical operator. (*a*) Trajectory of the unmodified self-sustaining state. (*b*) Trajectory of the stabilized self-sustaining state. Because this system is stable at every instance of time, it would asymptotically approach the zero perturbation state if its mean state time dependence were suppressed. This figure implies that the non-normal parametric mechanism maintains perturbation variance in both these self-sustaining states: (*a*) $R = 800$, $\sigma_r < 0.16$, $\langle \sigma_r \rangle = 0.045$; (*b*) $R = 800$, $\sigma_r < -0.001$, $\langle \sigma_r \rangle = -0.0011$.

Schmid & Henningson 1992; Reddy *et al.* 1998; Brandt *et al.* 2002). SSST analysis unites linear optimal theory with nonlinear perturbation/mean-flow interaction theory by showing that forcing of the streamwise roll by the perturbation field arises naturally from the robust process of turbulence organization by streaks. Moreover, in forced turbulence a finite-amplitude optimal or near-optimal perturbation would exist, at

least episodically, and such a perturbation would serve as an initial condition for the SSST streamwise roll and streak instability. We showed how the perturbation Reynolds stresses augment the growth of such an initial streamwise roll and streak. These processes cooperate in determining the structure of growing streamwise roll and streak perturbations. For this reason, comparison of SSST predictions with experiments requires accounting for both the amplitude and structure of initial perturbations as well as the growth rate of the SSST instability. If the level of forced turbulence is sufficiently high, an initially small-amplitude streamwise roll perturbation is converted into an unstable mode leading to transition. However, if the initial roll perturbation is large this unstable growth phase may be of less importance. After transition to the time-dependent state has occurred this state persists even if the turbulence is no longer externally forced. This mechanism of structural instability mediated transition to a self-sustaining state addresses the first problem mentioned above: transition from the laminar to the turbulent state in perturbation stable shear flow.

The streak spacing in the self-sustaining state is maintained through the parametric growth SSP mechanism, illustrated in figure 2. The streak spacing predicted by this parametric growth process is in agreement with observations of streak spacing of ~100 wall units in turbulent Couette flow. Before transition to the self-sustaining state the streamwise roll and streak growth is determined in part by the RGP mechanism, illustrated in figure 1. In Couette flow, the streamwise roll and streak spacing predicted by the RGP instability is approximately 50 wall units. There is no contradiction in the existence of these two scales of roll and streak organization given that the 50 wall unit spacing is associated with forced nearly laminar rolls and streaks while the 100 wall unit spacing is associated with the self-sustaining turbulent state.

The self-sustaining state studied here naturally evolved to a minimal turbulent system in which the dynamics is limited to the interaction of the streamwise-averaged flow with a single streamwise harmonic perturbation. This minimal turbulent system, which proceeds naturally from the SSST dynamics, provides a particular advantage for our study because the mechanism maintaining turbulence in this minimal system can be understood with clarity. In this self-sustaining state, we find that the streamwise roll is systematically maintained by the robust organization of perturbation Reynolds stress by the time-dependent streak while the streak is maintained by the streamwise roll through the lift-up mechanism. Systematic maintenance of the perturbation field results from the non-normal parametric growth mechanism arising from the interaction between the time-dependent streak and the perturbation. We hypothesize that this naturally emergent, minimal, self-sustaining, turbulent system captures the fundamental mechanism maintaining turbulence in wall-bounded shear flow.

Appendix. Optimal excitation of a mode in the energy norm

To determine the perturbation that excites optimally in energy a given eigenmode of the matrix $\boldsymbol{A}_k(\boldsymbol{U}_{eq})$, transform the perturbation state to $\hat{\boldsymbol{\psi}}_k = \boldsymbol{M}_k^{1/2}\hat{\boldsymbol{\phi}}_k$, with $\boldsymbol{M}_k$ the energy

metric defined in (3.12), so that the transformed dynamics become

$$\frac{\mathrm{d}\hat{\boldsymbol{\psi}}_k}{\mathrm{d}t} = \tilde{\boldsymbol{A}}_k \hat{\boldsymbol{\psi}}_k, \tag{A 1}$$

with $\tilde{\boldsymbol{A}}_k \equiv \boldsymbol{M}_k^{1/2} \boldsymbol{A}_k(\boldsymbol{U}_{eq}) \boldsymbol{M}_k^{-1/2}$. With this transformation, the perturbation energy density at streamwise wavenumber k, E_k in (3.13), is given simply by the inner product: $E_k = \hat{\boldsymbol{\psi}}_k^\dagger \hat{\boldsymbol{\psi}}_k$. The adjoint mode, $\hat{\boldsymbol{\psi}}_{k,a}$, of eigenmode $\hat{\boldsymbol{\psi}}_{k,m}$ of $\tilde{\boldsymbol{A}}_k$, is the eigenmode of $\tilde{\boldsymbol{A}}_k^\dagger$ with eigenvalue equal to the complex conjugate of the eigenvalue of $\hat{\boldsymbol{\psi}}_{k,m}$. It follows that $\hat{\boldsymbol{\psi}}_{k,b} \equiv \hat{\boldsymbol{\psi}}_{k,a}^*$ is the biorthogonal of $\hat{\boldsymbol{\psi}}_{k,m}$, that is, it is orthogonal to all of the other eigenmodes of $\tilde{\boldsymbol{A}}_k$. It can be shown that this perturbation structure excites the eigenmode $\hat{\boldsymbol{\psi}}_{k,m}$ optimally in energy (Farrell 1988; Farrell & Ioannou 1996*a*). Then, the optimal amplitude of excitation of the unit energy eigenmode $\hat{\boldsymbol{\psi}}_{k,m}$ resulting from a unit energy initial condition with the structure of its biorthogonal, $\hat{\boldsymbol{\psi}}_{k,b}$ is

$$a = \frac{1}{|\hat{\boldsymbol{\psi}}_{k,b}^\dagger \hat{\boldsymbol{\psi}}_{k,m}|}. \tag{A 2}$$

The ratio of the energy in the eigenmode resulting from excitation by this unit energy optimal, rather than direct excitation of the mode itself at unit energy, is a^2. For normal operators $a = 1$ while for highly non-normal operators, such as the evolution operator for a shear flow, this ratio is typically large.

REFERENCES

ADRIAN, R. J. 2007 Hairpin vortex organization in wall turbulence. *Phys. Fluids* **19** (4), 041301.

ALFREDSSON, P. H. & MATSUBARA, M. 1996 Streaky structures in transition. In *Proc. Transitional Boundary Layers in Aeronautics* (ed. R. A. W. M. Henkes & J. L. van Ingen). pp. 373–386. Royal Netherlands Academy of Arts and Sciences. Elsevier.

ANDERSSON, P., BERGGREN, M. & HENNINGSON, D. S. 1999 Optimal disturbances and bypass transition in boundary layers. *Phys. Fluids* **11**, 134–150.

ANDERSSON, P., BRANDT, L., BOTTARO, A. & HENNINGSON, D. S. 2001 On the breakdown of boundary layer streaks. *J. Fluid Mech.* **428**, 29–60.

BAKAS, N. A. & IOANNOU, P. J. 2011 Structural stability theory of two-dimensional fluid flow under stochastic forcing. *J. Fluid Mech.* **682**, 332–361.

BAKCHINOV, A. A., KATASONOV, M. M. & KOZLOV, V. V. 1997 Experimental study of localized disturbances and their development in a flat plate boundary layer. Preprint No. l-97, ITAM, Russian Academy of Sciences, Novosibirsk, Russia (in Russian).

BAMIEH, B. & DAHLEH, M. 2001 Energy amplification in channel flows with stochastic excitation. *Phys. Fluids* **13**, 3258–3269.

BATCHELOR, G. K. 2000 *An Introduction to Fluid Dynamics*. Cambridge University Press.

BENNEY, D. J. 1960 A nonlinear theory for oscillations in a parallel flow. *J. Fluid Mech.* **10** (02), 209–236.

BENNEY, D. J. 1984 The evolution of disturbances in shear flows at high Reynolds numbers. *Stud. Appl. Maths* **70** (02), 1–19.

BERKOOZ, G., HOLMES, P. & LUMLEY, J. L. 1993 The proper orthogonal decomposition in the analysis of turbulent flows. *Annu. Rev. Fluid Mech.* **25** (1), 539–575.

BERLIN, S. & HENNINGSON, D. S. 1999 A nonlinear mechanism for receptivity of free stream disturbances. *Phys. Fluids* **11** (02), 3749–3760.

BEWLEY, T. R. & LIU, S. 1998 Optimal and robust control and estimation of linear paths to transition. *J. Fluid Mech.* **365**, 23–57.

BRANDT, L., HENNINGSON, D. S. & PONZIANI, D. 2002 Weakly nonlinear analysis of boundary layer receptivity to free stream disturbances. *Phys. Fluids* **14**, 1426–1441.

BRANDT, L., SCHLATTER, P. & HENNINGSON, D. S. 2004 Transition in boundary layers subject to free stream turbulence. *J. Fluid Mech.* **517**, 167–198.

BUTLER, K. M. & FARRELL, B. F 1992 Three-dimensional optimal perturbations in viscous shear flows. *Phys. Fluids* **4**, 1637–1650.

CHAPMAN, S. J. 2002 Subcritical transition in channel flows. *J. Fluid Mech.* **451**, 35–97.

COSSU, C. & BRANDT, L. 2002 Stabilization of Tollmien–Schlichting waves by finite amplitude optimal streaks in the Blasius boundary layer. *Phys. Fluids* **14** (8), 57–60.

COSSU, C., BRANDT, L., BAGHERI, S. & HENNINGSON, D. S. 2011 Secondary threshold amplitudes for sinuous streak breakdown. *Phys. Fluids* **23** (7), 074103.

DELSOLE, T. 2004 Stochastic models of quasi-geostrophic turbulence. *Surv. Geophys.* **25**, 107–194.

DELSOLE, T. & FARRELL, B. F. 1996 The quasi-linear equilibration of a thermally mantained stochastically excited jet in a quasi-geostrophic model. *J. Atmos. Sci.* **53**, 1781–1797.

ELLINGSEN, T. & PALM, E. 1975 Stability of linear flow. *Phys. Fluids* **18**, 487–488.

FARRELL, B. F. 1988 Optimal excitation of perturbations in viscous shear flow. *Phys. Fluids* **31**, 2093–2102.

FARRELL, B. F. & IOANNOU, P. J. 1993*a* Optimal excitation of three-dimensional perturbations in viscous constant shear flow. *Phys. Fluids* **5**, 1390–1400.

FARRELL, B. F. & IOANNOU, P. J. 1993*b* Perturbation growth in shear flow exhibits universality. *Phys. Fluids* **5**, 2298–2300.

FARRELL, B. F. & IOANNOU, P. J. 1993*c* Stochastic dynamics of baroclinic waves. *J. Atmos. Sci.* **50**, 4044–4057.

FARRELL, B. F. & IOANNOU, P. J. 1993*d* Stochastic forcing of perturbation variance in unbounded shear and deformation flows. *J. Atmos. Sci.* **50**, 200–211.

FARRELL, B. F. & IOANNOU, P. J. 1993*e* Stochastic forcing of the linearized Navier–Stokes equations. *Phys. Fluids* A **5**, 2600–2609.

FARRELL, B. F. & IOANNOU, P. J. 1994 Variance maintained by stochastic forcing of non-normal dynamical systems associated with linearly stable shear flows. *Phys. Rev. Lett.* **72**, 1118–1191.

FARRELL, B. F. & IOANNOU, P. J. 1995 Stochastic dynamics of the midlatitude atmospheric jet. *J. Atmos. Sci.* **52**, 1642–1656.

FARRELL, B. F. & IOANNOU, P. J. 1996*a* Generalized stability. Part I. Autonomous operators. *J. Atmos. Sci.* **53**, 2025–2040.

FARRELL, B. F. & IOANNOU, P. J. 1996*b* Generalized stability. Part II. Non-autonomous operators. *J. Atmos. Sci.* **53**, 2041–2053.

FARRELL, B. F. & IOANNOU, P. J. 1998*a* Perturbation structure and spectra in turbulent channel flow. *Theor. Comput. Fluid Dyn.* **11**, 215–227.

FARRELL, B. F. & IOANNOU, P. J. 1998*b* Turbulence supresssion by active control. *Phys. Fluids* **8**, 1257–1268.

FARRELL, B. F. & IOANNOU, P. J. 1999 Perturbation growth and structure in time dependent flows. *J. Atmos. Sci.* **56**, 3622–3639.

FARRELL, B. F. & IOANNOU, P. J. 2003 Structural stability of turbulent jets. *J. Atmos. Sci.* **60**, 2101–2118.

FARRELL, B. F. & IOANNOU, P. J. 2007 Structure and spacing of jets in barotropic turbulence. *J. Atmos. Sci.* **64**, 3652–3665.

FARRELL, B. F. & IOANNOU, P. J. 2008*a* Formation of jets by baroclinic turbulence. *J. Atmos. Sci.* **65**, 3353–3375.

FARRELL, B. F. & IOANNOU, P. J. 2008*b* The stochastic parametric mechanism for generation of surface water waves by wind. *J. Phys. Oceanogr.* **38**, 862–879.

FARRELL, B. F. & IOANNOU, P. J. 2009 A stochastic structural stability theory model of the drift wave-zonal flow system. *Phys. Plasmas* **16**, 112903.

GAYME, D. F., MCKEON, B. J., PAPACHRISTODOULOU, A., BAMIEH, B. & DOYLE, J. C. 2010 A streamwise constant model of turbulence in plane Couette flow. *J. Fluid Mech.* **665**, 99–119.

GIBSON, J., HALCROW, J. & CVITANOVIĆ, P. 2008 Visualizing the geometry of state space in plane Couette flow. *J. Fluid Mech.* **611**, 107–130.

HALCROW, J., GIBSON, J. F., CVITANOVIC, P. & VISWANATH, D. 2009 Heteroclinic connections in plane Couette flow. *J. Fluid Mech.* **621**, 365–376.

HALL, P. & SHERWIN, S. 2010 Streamwise vortices in shear flows: harbingers of transition and the skeleton of coherent structures. *J. Fluid Mech.* **661**, 178–205.

HAMILTON, K., KIM, J. & WALEFFE, F. 1995 Regeneration mechanisms of near-wall turbulence structures. *J. Fluid Mech.* **287**, 317–348.

HERNON, D., WALSH, E. J. & MCELIGOT, D. M. 2007 Experimental investigation into the routes to bypass transition and the shear-sheltering phenomenon. *J. Fluid Mech.* **591**, 461–479.

HOEPFFNER, J. & BRANDT, L. 2008 Stochastic approach to the receptivity problem applied to bypass transition in boundary layers. *Phys. Fluids* **20**, 024108.

HOGBERG, M., BEWLEY, T. R. & HENNINGSON, D. S. 2003 Relaminarization of $Re = 1000$ turbulence using linear state-feedback control. *Phys. Fluids* **15**, 3572–3575.

HUTCHINS, N. & MARUSIC, I. 2007 Evidence of very long meandering features in the logarithmic region of turbulent boundary layers. *J. Fluid Mech.* **579**, 1–28.

HWANG, Y. & COSSU, C. 2010a Amplification of coherent structures in the turbulent Couette flow: an input–output analysis at low Reynolds number. *J. Fluid Mech.* **643**, 333–348.

HWANG, Y. & COSSU, C. 2010b Linear non-normal energy amplification of harmonic and stochastic forcing in the turbulent channel flow. *J. Fluid Mech.* **664**, 51–73.

JACOBS, R. G. & DURBIN, P. A. 2001 Simulations of bypass transition. *J. Fluid Mech.* **428**, 185–212.

JANG, P. S., BENNEY, D. J. & GRAN, R. L. 1986 On the origin of streamwise vortices in a turbulent boundary layer. *J. Fluid Mech.* **169**, 109–123.

JIMÉNEZ, J. & MOIN, P. 1991 The minimal flow unit in near-wall turbulence. *J. Fluid Mech.* **225**, 213–240.

JIMÉNEZ, J. & PINELLI, A. 1999 The autonomous cycle of near wall turbulence. *J. Fluid Mech.* **389**, 335–359.

JOVANOVIC, M. & BAMIEH, B. 2005 Componentwise energy amplification in channel flows. *J. Fluid Mech.* **534**, 145–183.

KAWAHARA, G. & KIDA, S. 2001 Periodic motion embedded in plane Couette turbulence: regeneration cycle and burst. *J. Fluid Mech.* **449**, 291–300.

KIM, J. & BEWLEY, T. R. 2007 A linear systems approach to flow control. *Annu. Rev. Fluid Mech.* **39**, 383–417.

KIM, J., KLINE, S. J. & REYNOLDS, W. C. 1971 The production of turbulence near a smooth wall in a turbulent boundary layers. *J. Fluid Mech.* **50**, 133–160.

KIM, J. & LIM, J. 2000 A linear process in wall bounded turbulent shear flows. *Phys. Fluids* **12**, 1885–1888.

KLEBANOFF, P. S., TIDSTROM, K. D. & SARGENT, L. M. 1962 The three-dimensional nature of boundary-layer instability. *J. Fluid Mech.* **12**, 1–34.

KOMMINAHO, J., LUNDBLADH, A. & JOHANSSON, A. 1996 Very large structures in plane turbulent Couette flow. *J. Fluid Mech.* **320**, 259–285.

KREISS, G., LUNDBLADH, A. & HENNINGSON, D. S. 1994 Bounds for threshold amplitudes in subcritical shear flows. *J. Fluid Mech.* **270** (1), 175–198.

KURIAN, T. & FRANSSON, J. H. M. 2009 Grid-generated turbulence revisited. *Fluid Dyn. Res.* **41**, 1–32.

LANDAHL, M. T. 1980 A note on an algebraic instability of inviscid parallel shear flows. *J. Fluid Mech.* **98**, 243.

LAVAL, J.-P., DUBRULLE, B. & MCWILLIAMS, J. C. 2003 Langevin models of turbulence: renormalization group, distant interaction algorithms or rapid distortion theory? *Phys. Fluids* **15**, 1327–1339.

LUCHINI, P. 2000 Reynolds-number-independent instability of the boundary layer over a flat surface: optimal perturbations. *J. Fluid Mech.* **404**, 289–309.

LUMLEY, J. L. 1967 The structure of inhomogeneous turbulence. In *Atmospheric Turbulence and Radio Wave Propagation* (ed. A. M. Yaglom & V. I. Tatarskii). pp. 166–178. Nauka.

MARSTON, J. B. 2010 Statistics of the general circulation from cumulant expansions. *Chaos* **20**, 041107.

MARSTON, J. B., CONOVER, E. & SCHNEIDER, T. 2008 Statistics of an unstable barotropic jet from a cumulant expansion. *J. Atmos. Sci.* **65**, 1955–1966.

MATSUBARA, M. & ALFREDSSON, P. H. 2001 Disturbance growth in boundary layers subjected to free stream turbulence. *J. Fluid Mech.* **430**, 149–168.

MONOKROUSOS, A., BOTTARO, A., BRANDT, L., DI VITA, A. & HENNINGSON, D. S. 2011 Non-equilibrium thermodynamics and the optimal path to turbulence in shear flows. *Phys. Rev. Lett.* **106**, 134502.

NAGATA, M. 1990 Three-dimensional travelling-wave solutions in plane Couette flow. *J. Fluid Mech.* **217**, 519–527.

NAGATA, M. 1997 Three-dimensional finite-amplitude solutions in plane Couette flow: bifurcation from infinity. *Phys. Rev.* E **55**, 2023–2025.

PEDLOSKY, J. & THOMSON, J. 2003 Baroclinic instability of time-dependent currents. *J. Fluid Mech.* **490**, 189–215.

POULIN, F. J., FLIERL, G. R. & PEDLOSKY, J. 2003 Parametric instability in oscillatory shear flows. *J. Fluid Mech.* **481**, 329–353.

POULIN, F. J., FLIERL, G. R. & PEDLOSKY, J. 2010 The baroclinic adjustment of time-dependent shear flows. *J. Phys. Oceanogr.* **40**, 1851–1865.

REDDY, S. C. & HENNINGSON, D. S. 1993 Energy growth in viscous shear flows. *J. Fluid Mech.* **252**, 209–238.

REDDY, S. C., SCHMID, P. J., BAGGETT, J. S. & HENNINGSON, D. S. 1998 On the stability of streamwise streaks and transition thresholds in plane channel flows. *J. Fluid Mech.* **365**, 269–303.

SCHLATTER, P., BRANDT, L., DE LANGE, H. C. & HENNINGSON, D. S. 2008 On streak breakdown in bypass transition. *Phys. Fluids* **20** (10), 101505.

SCHMID, P. J. & HENNINGSON, D. S. 1992 A new mechanism for rapid transition involving a pair of oblique waves. *Phys. Fluids* A: *Fluid Dyn.* **4**, 1986–1989.

SCHMID, P. J. & HENNINGSON, D. S. 2001 *Stability and Transition in Shear Flows*. Springer.

SCHOPPA, W. & HUSSAIN, F. 2002 Coherent structure generation in near-wall turbulence. *J. Fluid Mech.* **453**, 57–108.

SIROVICH, L., BALL, K. S. & KEEFE, L. R. 1990 Plane waves and structures in turbulent channel flow. *Phys. Fluids* A **2**, 2217–2226.

SMITH, C. R. & METZLER, S. P. 1983 The characteristics of low-speed streaks in the near-wall region of a turbulent boundary layer. *J. Fluid Mech.* **129**, 27–54.

SRINIVASAN, K. & YOUNG, W. R. 2012 Zonostrophic instability. *J. Atmos. Sci.* **69** (5), 1633–1656.

TOBIAS, S. M., DAGON, K. & MARSTON, J. B. 2011 Astrophysical fluid dynamics via direct numerical simulation. *Astrophys. J.* **727**, 127.

TREFETHEN, L. N., TREFETHEN, A. E., REDDY, S. C. & DRISCOLL, T. A. 1993 Hydrodynamic stability without eigenvalues. *Science* **261**, 578–584.

WALEFFE, F. 1995 Hydrodynamic stability and turbulence: beyond transients to a self-sustaining proccess. *Stud. Appl. Maths* **95**, 319–343.

WALEFFE, F. 1997 On a self-sustaining process in shear flows. *Phys. Fluids* A **9**, 883–900.

WALEFFE, F. 1998 Three-dimensional coherent states in plane shear flows. *Phys. Rev. Lett.* **81**, 4140–4143.

WALEFFE, F. 2001 Exact coherent structures in channel flow. *J. Fluid Mech.* **435**, 93–102.

WALEFFE, F. 2003 Homotopy of exact coherent structures in plane shear flows. *Phys. Fluids* **15**, 1517–1534.

WESTIN, K. J. A., BAKCHINOV, A. A., KOZLOV, V. V. & ALFREDSSON, P. H. 1998 Experiments on localized disturbances in a flat plate boundary layer. Part 1. The receptivity and evolution of a localized free stream disturbance receptivity and evolution of a localized free stream disturbance. *Eur. J. Mech.* (B/*Fluids*) **17**, 823–846.

WESTIN, K. J. A., BOIKO, A. V., KLINGMANN, B. G. B., KOZLOV, V. V. & ALFREDSSON, P. H. 1994 Experiments in a boundary layer subjected to free stream turbulence. Part 1. Boundary layer structure and receptivity. *J. Fluid Mech.* **281**, 193–218.

WU, X. & MOIN, P. 2009 Direct numerical simulation of turbulence in a nominally zero-pressure-gradient flat-plate boundary layer. *J. Fluid Mech.* **630**, 5–41.

ZHANG, Y. & HELD, I. M. 1999 A linear stochastic model of a GCM's midlatitude storm tracks. *J. Atmos. Sci.* **56**, 3416–3435.